2-Mercaptobenzimidazole derivative of chitosan for silver sorption – Contribution of magnetite incorporation and sonication effects on enhanced metal recovery

Khalid Elwakeel, Abdullah Al-Bogami, Eric Guibal

2-Mercaptobenzimidazole derivative of chitosan for silver sorption – Contribution of magnetite incorporation and sonication effects on enhanced metal recovery

Khalid Z. Elwakeel[a,b,1], Abdullah S. Al-Bogami[a,2], Eric Guibal[c,*,3]

[a] University of Jeddah, College of Science, Department of Chemistry, Jeddah, Saudi Arabia
[b] Environmental Science Department, Faculty of Science, Port-Said University, Port-Said, Egypt
[c] Polymers Composites and Hybrids (PCH), IMT Mines Ales, Alès, France

HIGHLIGHTS

- Synthesis of magnetic and non-magnetic mercaptobenzimidazole chitosan derivatives.
- Silver sorption is enhanced by sonication in terms of kinetics and thermodynamics.
- Selectivity for precious metals *vs.* base metals, especially in presence of EDTA.
- High desorption efficiency and stability of the sorbent at recycling.
- Highly efficient recovery of precious metals from acidic leachates of E-waste.

GRAPHICAL ABSTRACT

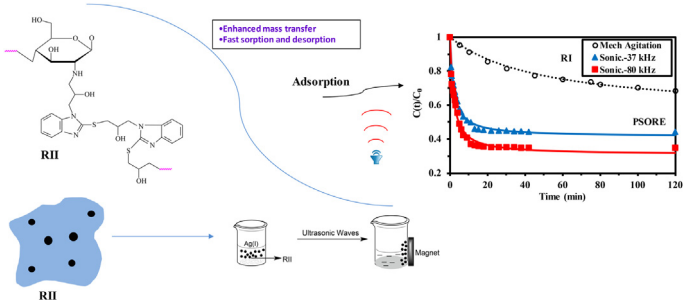

ABSTRACT

The recycling of precious and strategic metals from secondary resources (including E-wastes) is of critical importance for the recovery of scarce metals widely used in High-Tech devices. Therefore, the development of efficient and selective sorbents is of great importance. The grafting of 2-mercaptobenzimidazole onto chitosan microparticles allows developing highly selective sorbents. The incorporation of magnetite particles is also a strategic aspect for facilitating the use and recovery of microparticles. Sonication (at two different frequencies: 37 kHz and 80 kHz) shows high potential for improving both kinetic and thermodynamic aspects associated with silver uptake on 2-MBI-chitosan materials. Sorption capacities as high as 3 mmol Ag g^{-1} can be obtained with contact times as low as 20–30 min. The sorption isotherms are successfully fitted by the Langmuir and the Sips equations, while the kinetic profiles are modeled using the pseudo-second order rate equation and the resistance to intraparticle diffusion. The sorption process is exothermic: the sonication (and the frequency of sonic generator) strongly changes the thermodynamic parameters. The sonication also speeds up metal desorption, which is highly efficient using acidic thiourea solutions: the sonication allows also reducing the concentration of thiourea in the eluent required for complete silver elution. The sorbent shows remarkable stability is terms or sorption and desorption for five successive recycling runs. The acid leachates of printed circuit board are efficiently treated with the 2-MBI-chitosan sorbent for the recovery, enrichment and separation of precious metals (Ag, Au and Pd) from base metals (major elements: iron copper, aluminum, tin).

Keywords:
Functionalized chitosan
Silver enhanced sorption
Sonication-assisted sorption
Magnetic sorbent
Thermodynamics

* Corresponding author at: Polymers Composites and Hybrids (PCH), IMT – Mines Ales, Alès, France.
E-mail addresses: kelwkeel@uj.edu.sa (K.Z. Elwakeel), aalbogami@uj.edu.sa (A.S. Al-Bogami), eric.guibal@mines-ales.fr (E. Guibal).
[1] ORCID: 0000-0002-8853-284X.
[2] ORCID: 0000-0002-8670-2729.
[3] ORCID: 0000-0002-2767-6305.

1. Introduction

The development of high-tech devices induces increasing demand on precious and strategic metals (such as metals from the "platinum mine", silver, and rare earth elements). The resources limitations and the environmental impact of the extraction of these strategic metals are two strong incentives for their recycling from secondary sources such as wastes electrical and electronic equipment (WEEE) [1,2]. For example, European Union has promoted several regulations for WEEE valorization and recycling [3]. Resource saving and environment preservation may explain the increasing research for the beneficiation of valorizable metals from waste materials [4,5]. Thermal treatments (roasting), organic/inorganic and magnetic separations are preliminary steps in the general process of beneficiation [6]. However, hydrometallurgy remains one the most frequent strategies for metal recovery; involving leaching process for metal recovery from solid wastes [7,8]. The removal of metals from leachates may involve different processes such as solvent extraction [8–12], associated with electro-winning and redox processes [13,14], especially when the concentrations are high enough to make these processes competitive. For more dilute solutions (containing less than 200 mg Ag L^{-1}), sorption processes may be more appropriate. These processes may also efficiently contribute to the other important challenge of selective separation of precious metals. The selectivity may be direct (i.e., removing preferentially silver) or indirect (purifying silver solutions from other noble metal impurities). For example, Musina et al. [15] reported the attractive selectivity of phosphine-oxide bearing resin (MPX-310 resin) for platinum and palladium from silver and copper electrolyte solutions.

In the case of thiosulfate leachates, silver was efficiently recovered using quaternary ammonium based-sorbents (quaternary PEI/PAN, and Amberlite IRA-458 resin) [16]. Phosphorus-based resins were also reported as promising sorbents for Ag(I) in nitric acid solutions. Villemin et al. [17] prepared phosphonate-polyethyleneimine resins (PEI), by controlled reaction of phosphorous acid with PEI, for preparing ion-exchange resins and Ag-based antimicrobial polymers. A series of imidazole-based and polyamine resins was designed for the sorption of silver from HCl solutions [18]: imidazole-based resins reveal more efficient than polyamine-based resins.

Sulfur-based resins have also been frequently reported for their high affinity for silver ions [19,20]; for example, thiourea was grafted on chloromethylated polystyrene for silver binding from nitrate solutions [21], while Hao et al. [22] reported the efficient syntheses of different thiourea-formaldehyde resins with out-standing sorption properties for Ag(I) (i.e., higher than 22 mmol Ag g^{-1}). Yun et al. [23] described the synthesis of a highly-stable thiourea derivative of polystyrene for enhanced sorption of silver (about 1.76 mmol Ag g^{-1}). Dithioxamide (DTA), bearing two amine groups and two sulfur groups, was successfully immobilized on polysiloxane-based resins (0.9 mmol DTA g^{-1}) for silver sorption (up to 5 mmol Ag g^{-1}) [24]. Magnetic polypyrrhole nanocomposites have been functionalized by thiol grafting; maximum sorption capacity reached up to 7.47 mmol As g^{-1} [25]. Trithiocyanuric-functionalized poly(glycidylmethacrylate) microbeads were also used for Ag(I) uptake [26].

Chitosan-based materials offer interesting perspectives for chemical modification and synthesis of functionalized materials because of the presence of highly reactive groups (–OH, amine groups) [27–31]. In addition, chitosan can be also readily conditioned as magnetic composite for readily separation of micro- and nanoparticles from aqueous solutions. Indeed, microparticles allows improving kinetics (shortening the path for intraparticular diffusion) and substantially reducing equilibrium times [32–34].

Sulfur- and imidazole-based resins have been reported above for their efficient chelation of precious metals [35]. 2-Mercaptobenzimidazole (MBI) combines sulfur and imidazole groups and develops attractive binding properties that were used for synthesizing new resins [36–41].

Based on the high potential of chitosan for magnetite incorporation and for functionalization and the high reactivity of MBI, the current research focused on the grafting of MBI on chitosan polymer. The sorbent is declined as non-magnetic (RI) and magnetic (RII) resins. The sorption properties are investigated in a first step for synthetic silver-nitrate solutions through the study of pH effect, uptake kinetics, sorption isotherms and desorption performance (kinetics and recycling) for the two sorbents. Previous studies have shown the strong enhancement of uptake kinetics when sonication is associated with the sorption step [42–45]. Therefore, the uptake kinetics and sorption isotherms are systematically compared using mechanical agitation (MA) and ultrasonic treatment (UT) applied under two different frequencies (F1: 37 kHz and F2: 80 kHz). In a second step, sorption is investigated in binary solutions in acidic solutions to prepare the application of the sorption process to silver recovery from leachates of E-waste (electronic waste). The presence of heavy metals in addition to other precious metals (gold and palladium) is investigated also in the presence of EDTA, used a masking agent. Finally, the recovery of silver and palladium is studied in a real E-waste leachate considering both the sorption and the desorption steps, using R1 sorbent under UT-F1 agitation. To the best of our knowledge, this is the first time a 2-mercaptobenzimidazole-derivative of chitosan is tested for silver sorption and applied for the treatment of real E-waste acidic leachates. The contribution also thoroughly investigates the relative contributions of the incorporation of magnetite core and sonication in the enhancement of sorption and desorption performances (both in terms of mass transfer and thermodynamic aspects).

2. Materials and methods

2.1. Materials

Chitosan, 2-mercaptobenzimidazole (2-MBI), epichlorohydrin (99% w/w), Ammonium iron(III) sulfate dodecahydrate ($(NH_4)Fe(SO_4)_2{\cdot}12H_2O$) and iron(II) sulfate ($FeSO_4{\cdot}7H_2O$)were provided by Sigma-Aldrich (Merck, Darmastadt, Germany), as analytical grade reagents. $AgNO_3$, $Au(NO_3)_3$, $Pd(NO_3)_2{\cdot}2H_2O$, $Cu(NO_3)_2{\cdot}3H_2O$, $Al(NO_3)_3{\cdot}9H_2O$, $Fe(NO_3)_3{\cdot}9H_2O$, $Sn(NO_3)_2$, $Pb(NO_3)_2$, $Ni(NO_3)_2$, $Zn(NO_3)_2$ were purchased from Sigma-Aldrich (Darmstadt, Germany).

2.2. Synthesis of sorbents

2.2.1. Synthesis of magnetite nanoparticles

Magnetite nanoparticles were synthesized by the hydrothermal co-precipitation of ferric and ferrous salts [46]. Firstly, $FeSO_4{\cdot}7H_2O$ (5.0 g) and $(NH_4)Fe(SO_4)_2{\cdot}12H_2O$ (17.35 g) were dissolved in 400 mL of demineralized water. The as-dissolved iron mixture was heated under reflux (333 ± 1 K) in a 1.0 L flask. The mixture was magnetically stirred for 60 min under N_2 atmosphere. Then, NaOH (3 M) solution was slowly and progressively added to the mixture until pH reached 12; the reaction took place at 318 K for 5 h. The magnetite particles were magnetically separated and washed repeatedly with Milli-Q water (Millipore, Billerica, MA, USA) until the suspension reached a pH close to 7. Finally, the solid was rinsed with acetone, and dried, under

vacuum, at 333 ± 1 K, for 5 h.

2.2.2. Synthesis of RI sorbent (Scheme 1a)

Chitosan (5.6 g) and 2-mercaptobenzimidazole (6.1 g) were suspended in 250 mL Milli-Q water; the mixture was stirred for 30 min at 1000 rpm in a 500-mL two-necked round-bottomed flask. In a second step, 4.75 mL of epichlorohydrin was added from the side opening, under stirring at 1000 rpm. The suspension was heated at 70 °C for 3 h. The yellow product (RI) was recovered by filtration and carefully washed (for removing unreacted reagents) and finally dried under vacuum for 6 h at 323 ± 1 K. The synthesis was almost quantitative: the yield was close to 98.8% (i.e., 17.1 g of product for a total of 17.3 g of precursors). The proposed chemical structure of RI is shown in Scheme 1a.

2.2.3. Synthesis of RII sorbent (Scheme 1b)

Magnetic chitosan particles were prepared by dissolving chitosan (5.6 g) in 200 mL of diluted acetic acid (~7%, w/w). After complete dissolution of chitosan, 2.5 g of previously prepared Fe_3O_4 were add to the flask under continuous stirring (at 1000 rpm). Sodium hydroxide (0.5 M) was added drop by drop until complete precipitation of magnetic chitosan. The product was washed several times with Milli-Q water. Washed magnetic chitosan was dropped into 250 mL of Milli-Q water (in a 500-mL two-necked round-bottomed flask). In the next step, 2-mercaptobenzimidazole (6.1 g) and additional magnetite (2.5 g) were added in the reactor under agitation for 30 min. Next, epichlorohydrin (4.75 mL) was added from the side opening under stirring at 1000 rpm. The suspension was heated at 70 °C for 3 h. A black product (i.e., RII) was recovered by filtration and magnetic separation. Unreacted reagents were carefully washed up with water, and the sorbent was finally dried under vacuum for 6 h at 50 ± 1 °C. The yield of the magnetic sorbent was close to 98.2% (i.e., 21.9 g of product for a total of 22.3 g of reagents).

2.3. Characterization of materials

Fourier-Transform infrared spectra were acquired using a Nicolet IS10 FTIR (Thermo Fisher Scientific, Waltham, MA, USA) equipped with an ATR accessory (attenuated total reflectance). The surface area and pore analysis of the sorbent particles (BET surface, pore volume and pore size) were performed using a Quantachrome NOVA 3200e (Quantachrome Instruments, Boynton Beach, FL, USA); the data were analyzed using NovaWin software (v11.0). Thermogravimetric analysis was operated on a Shimadzu TGA-50 thermogravimetric analyzer (Shimadzu Corporation, Tokyo, Japan). The surface charge measurements of the sorbent (zeta potential) were performed using a Nano Zeta Sizer (Nano-ZS Malvern Instruments Ltd., London, United Kingdom) at various pH values (from 2.02 to 12.02). The sorbent particles (0.01 g) were suspended in 50 mL of 0.1 M KCl solution for 2 h before analysis. Transmission electron microscope (TEM-2100HR, JEOL, Tokyo, Japan) was used for the ultrahigh resolution analysis of magnetite nanoparticles, the particles were suspended in demineralized water before being spread on carbon grids. Magnetization tests were carried out at room temperature using a vibrating sample magnetometer (VSM, Princeton Measurements Corporation, PMC MicroMag 3900 model, Princeton, NJ, USA), applying a maximum magnetic field of 10 kOe.

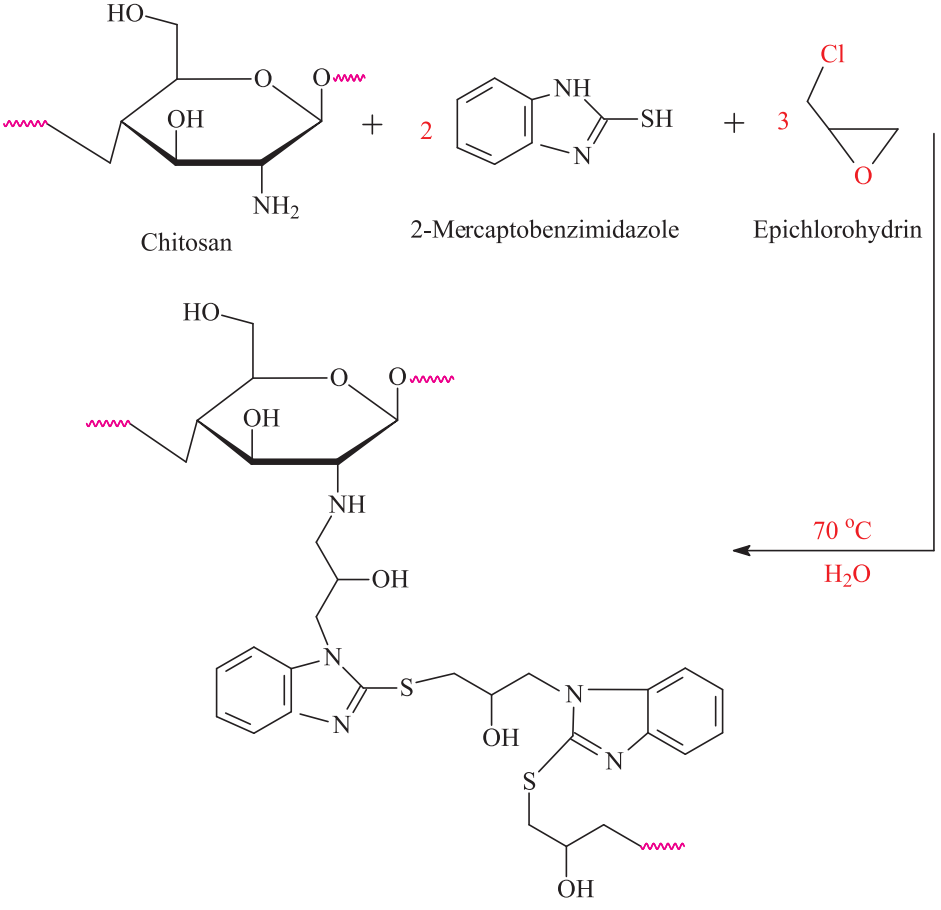

Scheme 1a. Synthesis pathway and proposed structure of 2-MBI functionalized chitosan (RI sorbent).

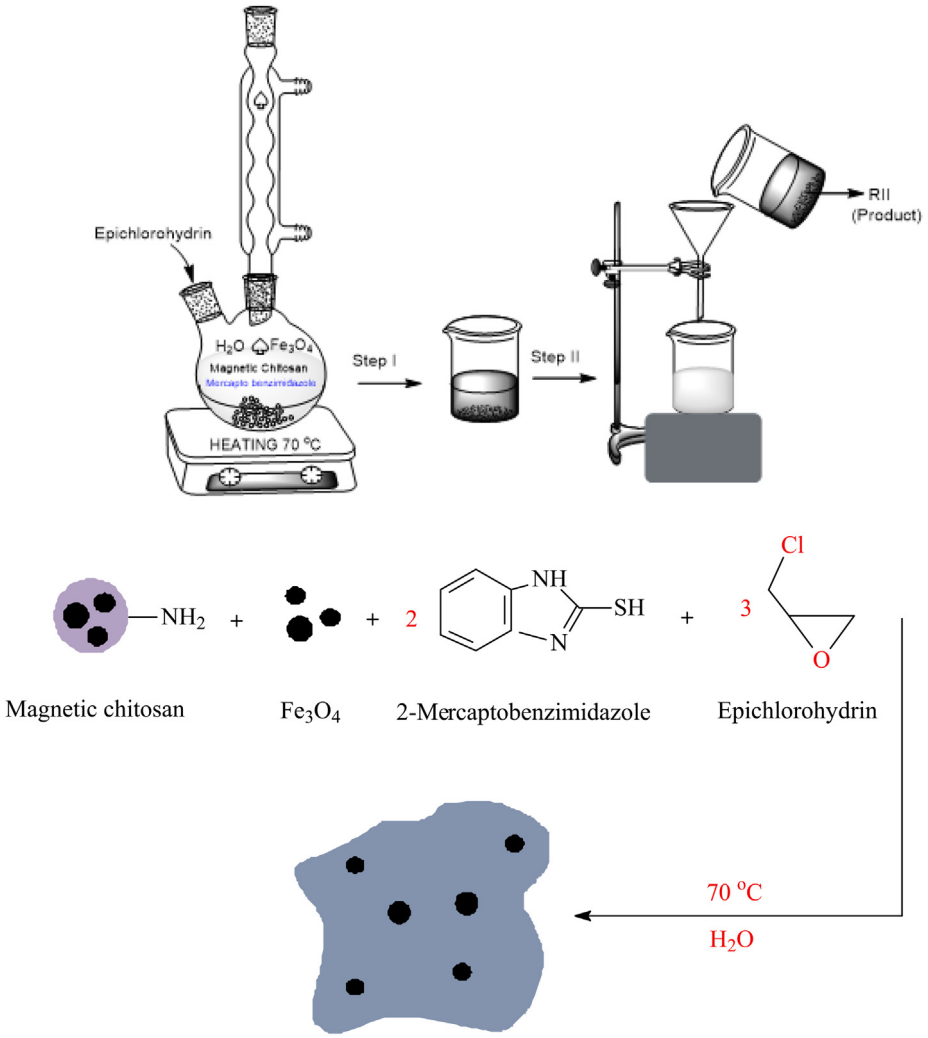

RII

Scheme 1b. Synthesis pathway for the preparation of RII sorbent.

The sizes of sorbents microparticles and magnetite nanoparticles were analyzed by differential light scattering using a DLS particle size analyzer NanoBrook 90Plus (Brookhaven Instruments Corporation, Holtsville, NY, USA).

2.4. Sorption tests

Stock solutions of 0.01 M Ag(I) ions were prepared by dissolving silver nitrate salt; the working solutions were prepared by dilution of the stock solution with ultrapure water (Milli-Q), just prior experiments.

2.4.1. pH effect

The influence of the pH on Ag(I) uptake was investigated by contact of 20 mL (V) of Ag(I) solution (C_0: 10.0 mmol Ag L^{-1}) with 0.02 g of sorbent (m, dry weight); the sorbent dosage (SD) was usually set at 1 g L^{-1}. For mechanical agitation (MA) tests, sorption experiments were performed using a shaking incubator (LSI-3016R, Labtech, Sorisole (BG), Italy) at room temperature (i.e., 298 ± 1 K), unless specified. The value of initial pH was varied between 1.12 and 7.08 using HNO_3 (0.0001–0.01 M) or NaOH (0.0001 M). The pH before and after sorption were measured using a pH meter (HANNA 211, Hanna Instruments, Lingolsheim, France). The suspension was stirred under an agitation speed of 210 rpm for 6 h. After contact, the sorbents were separated from the solutions by filtration for RI using filter membranes (Whatmann, Merck, Kenilworth, NJ, USA) or by magnetic separation for RII. The filtrates were analyzed for residual Ag(I) concentration using an inductively coupled plasma mass spectrometer (ICP-MS, Elan 9000, Perkin Elmer, USA). The duplication/triplication of selected sorption experiments were performed to ensure that the standard deviations are in an acceptable range (see examples in Annex on repeatability tests in Supplementary Information).

2.4.2. Uptake kinetics

For uptake kinetics, a fixed amount of sorbent was mixed with a fixed volume of Ag(I) solution (sorbent dosage, SD: 1 g L^{-1}) at pH 6.8. Samples (4 mL) were collected (by filtration or magnetic separation for RI and RII, respectively) at fixed time intervals, then the residual concentrations of Ag(I) were determined by ICP-MS. For mechanical sorption, the agitation speed was set at 210 rpm, while the temperature was maintained at 298 ± 1 K. In order to investigate the influence of ultrasonic treatment on the sorption of Ag(I), the sorption experiments were conducted under the same conditions. The unique difference consisted of using an ultrasonic bath sonicator (Elmasonic P300H ultrasonic bath, continuous mode, with power: 380 W). Two different frequencies were tested for ultrasonic treatment (UT) corresponding to

frequency F1: 37 kHz, and F2: 80 kHz; the temperature was controlled using a thermostatic box. The sorbed amount of Ag(I) per unit weight of the sorbent at time t ($q_{(t)}$, mmol Ag g^{-1}) was calculated from the following mass balance equation (taking into account the decrement in the volume of the solution).

$$q_{eq} = \frac{(C_0 - C_{eq})V}{m} \quad (1)$$

2.4.3. Sorption isotherms

Mechanical agitation sorption isotherms were obtained by contact of 0.02 g of sorbent (m) with a fixed volume of solution (V = 20 mL) of Ag(I) solution at different initial concentrations (C_0, ranging between 1.0 and 10.0 mmol L^{-1}) for 6 h. The pH of the solutions was initially set at 6.8, after solid/liquid separation. The same tests were performed using sonication (UT-F1 and UT-F2). The equilibrium pH and the residual metal ion concentration (C_{eq}, mmol Ag(I) L^{-1}) were systematically measured; the amount of sorbed metal ions (q_e, mmol g^{-1}) was estimated by the mass balance.

The effects of mechanical agitation and sonication on Ag(I) uptake were investigated at pH_0 6.8, for different temperatures (25 °C, 35 °C , 45 °C and 55 °C; temperature variation did not exceed 1 °C, compared to set value). After solid/liquid separation, the residual concentrations (C_{eq}, mmol L^{-1}) were determined and the sorption capacities (q_{eq}, mmol g^{-1}) were calculated using the mass balance equation.

Selective extraction of Ag(I) from binary mixtures with Cu(II), Pb (II), Cd(II), Zn(II) or Ca(II) was studied at pH 2 using RI and RII sorbents. A fixed amount of dry sorbent (i.e., 0.02 g) was mixed with 20 mL of 2 mmol L^{-1} Ag(I) solution in a binary mixture with 2 mmol L^{-1} Au(III), Pd(II), Cu(II), Al(III), Fe(III), Sn(II), Pb(II), Ni(II) and Zn(II) in absence and presence of 4 mmol L^{-1} EDTA. These experiments were performed under sonication (Frequency: 37 kHz, UT-F1) for 30 min. The residual concentrations of Ag(I) and of the competitor metal ion were determined by ICP-MS.

2.4.4. Metal desorption

After being loaded, the sorbents were washed with ultrapure water and dried. The mass balance equation was used to quantify the effective amount of Ag (I) ions immobilized on the sorbents (i.e., 2.25/2.79/3.25 mmol Ag g^{-1} RI and 1.86/2.65/3.11 mmol Ag g^{-1} RII, loadings under MA, UT-F1 and UT-F2, respectively). A fixed amount of metal-loaded sorbent was mixed with a fixed volume of acidic thiourea solutions (SD: 1 g in 20 mL) with increasing concentrations (0.2–0.8 mol L^{-1}) (pH 2 in for RI and pH 4 for RII). Samples were collected at fixed times for evaluating the desorbed amounts of Ag(I) ions and plotting the desorption kinetics. The desorption process was performed in a shaking incubator at 210 rpm and under different ultrasound frequencies of 37 kHz (UT-F1) and 80 kHz (UT-F2). All desorption experiments were performed at room temperature (i.e., 25 ± 1 °C). One-mL samples were collected at different time intervals from desorption medium to analyze the kinetic profile of desorption process. Thereafter, the regenerated sorbents were collected (by filtration for RI; magnetically for RII), then carefully washed by ultrapure water for reuse in the next run. The desorption efficiency at time t (DE, %) was calculated according to the following equation:

$$DE(\%) = \frac{\text{Amount of desorbed Ag(I) (mmol) into the eluate at time t}}{\text{Amount of sorbed Ag(I) (mmol) at equilibrium}} \times 100 \quad (2)$$

2.4.5. Sorption modeling

Conventional equations were used for modeling uptake kinetics and sorption isotherms. Table S1a (see Supplementary Information) reports the pseudo-first order rate equation (PFORE), the pseudo-second order rate equation (PSORE) and the resistance to intraparticle diffusion (RIDE, Crank equation) for uptake kinetics. Table S1b summarizes the equations for Langmuir, Freundlich, Sips and Temkin equations used for fitting sorption isotherms. The facilities of Mathematica® were systematically used for non-linear regression analysis and determination of model parameters.

Note: full experimental conditions are systematically reported in the caption of the figures and tables.

2.5. Application to WEEE leachate

2.5.1. Leachate production

The study was performed using electronic wastes with high silver content. The electronic components were manually separated from printed circuit board (PCB), leaving only the substrate with traces of welding. To remove some components such as electrolytic aluminum capacitors, resistors, heat sinks, and connection peripherals from the PCB, a milling was performed, and the grinded PCB was classified by particle size. This pre-treatment was followed by magnetic separation of ferrous fractions, including steel. Acidic leaching solutions were prepared in Milli-Q water using analytical grade chemicals. The smallest fraction size (1.5–3 mm) of grinded PCB (50 g) was leached with 100 mL of 2 mol L^{-1} H_2SO_4 and 44 mL of 15% (v/v) H_2O_2 at 75 °C for 1 h under agitation (at 250 rpm) [47]. The undissolved plastics were removed from the leachate using colander; then 50 mL of nitric acid 2 mol L^{-1} was added under agitation at 250 rpm for 1 h at 70 °C to displace the speciation of metal ions and form soluble nitrate species. Finally, the pH was adjusted at pH 2, adding NaOH (0.5 M) drop wise. The concentrations of Ag(I), Au(III), Pd(II), Cu(II), Al(III), Fe(III), Sn(II), Pb(II), Ni(II) and Zn(II) in the pre-treated leachate were determined by ICP-MS.

2.5.2. Sorption tests

Silver ion separation from the pregnant leach liquor (PLL) containing Au, Pd, Cu, Al, Fe, Sn, Pb, Ni and Zn was tested using RI sorbent in batch reactor, using sonication at 35 kHz frequency (UT-F1) for agitation. Experimental conditions correspond to pH_0: 1.95; pH_{eq}: 2.76; SD: 1 g L^{-1}; T: 25 ± 1 °C; contact time: 15 min. The desorption of metal ions from the loaded sorbent was performed using 0.8 M acidified thiourea solution (pH 2) applying the following experimental conditions: SD: 1 g sorbent/20 mL eluent; T: 25 ± 1 °C; contact time: 10 min; agitation mode: UT-F1, 37 kHz frequency.

3. Results and discussion

3.1. Characterization of materials

3.1.1. Textural properties

Fig. S1 (see Supplementary Information) shows TEM images for magnetite nanoparticles, they are characterized by a large variety of size (8–45 nm) and morphology (cubic and rounded particles). The DLS analysis of magnetite microparticles demonstrates that magnetite tends to agglomerate to form objects with size in the range 2–20 μm (Fig. S2). Both RI and RII particles have a size distribution in the range ~200–750 μm; the peak fraction corresponds to ~486 μm for RI and ~560 μm for RII. The incorporation of magnetite slightly increases the size of composite material.

Table 1 summarizes the textural properties of the two resins. Fig. S3 compares the nitrogen sorption and desorption isotherms of RI and RII materials. The specific surface areas (SSA) are limited to 8.0 and 4.8 m^2 g^{-1}. This decrease in SSA between RI and RII is consistent with the increase in their average size. Raw chitosan is generally considered a poorly porous polymer (specific surface area counting for a few m^2 g^{-1}); surprisingly, the entrapment of magnetite nanoparticles decreases the specific surface area of the composite. Tanhaei et al. [48] reported higher SSA values for magnetic chitosan particles (i.e., close to 22 m^2 g^{-1}). Hosseini et al. [49] synthesized a series of magnetic and chitosan

Table 1
Textural properties of RI and RII sorbents.

Parameter	Sorbent	
	RI	RII
Specific surface area ($m^2\ g^{-1}$)[a]	8.076	4.843
Total Pore volume ($cm^3\ g^{-1}$)[b]	0.033	0.021
Average pore diameter (nm)	24.523	35.588
Average particle size (μm)	486.23	560.51

Note: Average particle size of magnetite microparticles (used for the synthesis of sorbent): 8.8 μm.

based materials; they found specific surface area in the range 45–50 $m^2\ g^{-1}$. The composite materials showed an increase in the external surface area compared with raw magnetite particles. The weak SSAs of RI and RII sorbents are confirmed by low values for porous volume (0.033 and 0.021 $cm^3\ g^{-1}$, respectively). The average pore diameter increases with the incorporation of magnetite nanoparticles. Both RI and RII can be qualified as mesoporous sorbents according IUPAC classification [49]. This is consistent with the hysteresis loop in N_2 adsorption and desorption isotherms.

3.1.2. VSM

The magnetization saturation (M_s) of Fe_3O_4 nanoparticles is close to 50 emu g^{-1} (Fig. S4); it is lower than the value reported for magnetite by Hosseini et al. [49] (i.e., 78 emu g^{-1}). The incorporation of the magnetic particles into functionalized chitosan strongly reduces the magnetization saturation to 13.4 emu g^{-1}. Hosseini et al. [49] observed that the direct functionalization of magnetite nanoparticles with amine groups decreased the M_s to 58 emu g^{-1}. However, the largest decrease resulted from the encapsulation of amino-functionalized Fe_3O_4 particles with carboxylated chitosan nanoparticles: the M_s value decreased to 30 emu g^{-1}. The polymer coating being non-magnetic, the encapsulation reduces the effective fraction of magnetite NPs in the composite, which, in turn, exhibits lower magnetization [50]. In the case of RII sorbent, the M_s value decreases by 73%. This decrease is consistent with the weight loss observed at 600 °C, corresponding to the thermal degradation of polymer coating (see Section 3.1.3. TGA): the weight loss was close to 71.3% compared with 91% for non-magnetic sorbent (i.e., RI); the magnetic fraction is close to 20%. The loss of magnetization is partially explained by the relative decrease of magnetic fraction in the composite but also to a lesser extent to the screening of polymer layer. In the insert of Fig. S5, the slope of the Moment/Mass plot *vs.* magnetic field is vertical for magnetite at low magnetic field; this is usually associated with superparamagnetic behavior. The coating of magnetite NPs notably decreases this slope showing the global depreciation of magnetization properties for the composite. However, this residual M_s is sufficient to readily separate magnetic sorbent from aqueous solution using an external magnetic field.

3.1.3. TGA

The thermal degradation of RI and RII sorbents is summarized in Fig. S5: the weight loss (TGA, %) and DrTGA (mg s^{-1}) are compared for the two materials, showing similar degradation steps. The first step corresponds to the loss of absorbed water (about 6.7%) up to a temperature of 130–140 °C. This phase corresponds also to DrTGA valleys at 56.64 °C for RI and 78.01 °C for RII. The second step is marked by a steep additional weight loss (~30% for RI and ~25% for RII) up to 280–290 °C; deep DrTGA valleys are identified at 242.97 °C and 250.58 °C for RII and RI, respectively. This step can be associated with the degradation of substituents on chitosan backbone. These first two steps are very close for the two sorbents; the shift is more marked for the final degradation path. The third phase corresponds to a progressive weight loss (total weight loss 57% for RI and 48% for RII) up to temperatures ~440 °C for RI and ~440 °C for RII. This phase corresponds to the depolymerization of the biopolymer and the char formation. The last section corresponds to the char degradation and to the phase transition of Fe_3O_4 to α-Fe_2O_3 (up to 630 °C) [51]. For RII, the phase transition of magnetite is probably associated with the valley observed at 531.73 °C; this valley almost masks the two valleys observed at 487 °C and 552.36 °C for RI.

Based on the variation of final weight loss (close to 20%) for RI and RII materials, the magnetite fraction can be roughly evaluated close to 20%, which is lower than the expected levels based on the amount of magnetite NPs introduced in the formulation of RII.

3.1.4. Zetametry

The zetametry analysis shows that the ζ-potential profiles are very close for RI and RII sorbents (pH_{PZC}: 8.30 and 8.23, respectively) (Fig. S6). The coating of magnetite nanoparticles completely inhibits the possible contribution of iron oxide to the surface charge of the sorbent. Foye and Lo [52] reported two pK_a values for 2-mercaptobenzimidazole at 9.80 and 2.60. More recently, Jerez et al. [53] investigated the pK_a values of a series of protonated benzimidazole derivatives (including 2-MBI): the pK_a values range between 4.48 and 7.38 (5.70–5.78 for 2-MBI). Pourreza et al. [54] reported the amphiprotic behavior of 2-MBI, which is characterized by two basic amine groups and an acidic-SH group (whose pK_a value was reported close to 9.97). The pK_a value for amine groups on chitosan strongly depends on the degree of acetylation of the biopolymer but for most commercial sources (with deacetylation degree higher than 80%) the pK_a is in the range 6.3–6.5 [55]. The pH_{PZC} of chitosan was evaluated to 6.5 [56]. The pH_{PZC} of the sorbents is thus the result of combined effects of the amine groups of chitosan and reactive functions hold on 2-MBI. This also means that in neutral and acidic solutions, the global charge of the sorbents is positive; this may influence the electrostatic attraction/repulsion effect of the sorbents for metal ions. The pH_{PZC} of 2-MBI impregnated clays was found much lower (close to 3.2) [41]. In the case of hydrotalcite impregnation with 2-MBI, Anirudhan et al. [40] reported a pH_{PZC} value close to 5.

3.1.5. Elemental analysis

Table S2 summarizes the CHNS analysis of both RI and RII sorbents. As expected, the incorporation of magnetite nanoparticles in RII reduces the content of N and S elements. The S content is the tracer of 2-MBI grafting on the composite material. The sulfur content varies between 2.44 and 2.95 mmol S g^{-1} for RII and RI, respectively. This is a clear evidence for the successful immobilization of 2-MBI on chitosan. Based on the actual content of S and the theoretical stoichiometry between S and N in the grafted material (i.e., 2 nitrogen from 2-MBI and 1 nitrogen from chitosan [57]), the expected N content should be 8.85 and 7.32 mmol N g^{-1} for RI and RII, respectively. The elemental analysis shows an excess of S content compared with N content. The binding of one unit of 2-MBI per chitosan unit is thus poorly probable. The synthesis procedure differs from the method described by Sharma et al. [57]; it may explain the unexpected low N/S ratio.

3.1.6. FTIR spectrometry

Fig. S6 compares the FTIR spectra of RI and RII sorbents on selected wavenumber ranges. The usual characteristic peaks of chitosan are identified on the spectra (Table S3), such as the carbohydrate ring (in the range 1200–800 cm^{-1}), the amide bands (for non-fully deacetylated chitosan around 1650 cm^{-1} and 1626 cm^{-1}), the amine bands (at 1558 cm^{-1}) [58]. Some of these assignments are difficult to identify due to cross-contributions associated with 2-MBI (nitrogen from imidazole groups, proper C–H groups in the specific environment of imidazole ring, etc.). Some sulfur groups are identified [57]; for example at ~2350 cm^{-1} (weak signals, associated with S-H stretching), C-S stretching (around 740 cm^{-1}) or S-O (around 613 cm^{-1}, [40]). The method of Sharma et al. [57] consists of the impregnation of chitosan with 2-MBI in acetone medium. This method differs from the chemical grafting used for the preparation of RI and RII; it may explain the shift

of some of these specific sulfur and amine vibrations. Anyway, the appearance of these specific peaks confirms the elemental analysis and the successful grafting of 2-MBI onto chitosan supports (RI and RII). The poorly resolved peak appearing 568 cm^{-1} for RII confirms the presence of magnetite-based material in the sorbent [59]. On the other side, the important shift of the band around 3400–3300 cm^{-1} for RII sorbent is directly correlated with the presence of magnetite that brings the important contribution of OH associated with iron oxides. This band hides the small shoulder appearing on RI sorbent at 3110 cm^{-1}, which was identified on 2-MBI [60].

3.2. Sorption studies

3.2.1. Effect of pH

Fig. 1 shows the progressive and linear increase of Ag(I) sorption capacity with the equilibrium pH. The pH may affect metal ion binding through different mechanisms: (a) metal speciation, (b) ionization of reactive groups at the surface of the sorbent, and (c) the apparent affinity of reactive groups for metal ions. In the case of silver ions in nitric acid solutions, the predominant form of metal ions is free Ag^+. In the range pH 2–7, free Ag^+ represents more than 99% of total species; at pH below 2, a small fraction of silver is present as $AgNO_3$ (5.75% at pH 1 and up to 14.35% at pH 0.5). This weak variation in metal speciation with pH clearly demonstrates that the pH effect is associated to other criteria. The curves are parallel for RI and RII (with a slope close to 0.16–0.17); the same reactive groups at the surface of the two sorbents may explain this similitude. The ordinate intercept decreases from 0.68 mmol Ag g^{-1} for RI to 0.41 mmol Ag g^{-1} for RII. The incorporation of magnetite nanoparticles in the composite sorbent (i.e., RII) obviously decreases the proportion of active material. The expected amount of magnetite in the composite is 20–30%; this is lower than the observed decrease in sorption capacity (about 40%). The pH_{PZC} of the two sorbents is close to 8.30–8.23. This means that in the investigated pH range (i.e., 1–7 for pH_{eq}) the surface of the sorbents is globally positive. This also means that silver ions may be electrostatically repulsed by the high positive charge of the sorbents. Similar conclusions have been reported for Ag(I) sorption onto hollow chitosan beads [61]. With the increase of the pH, this repulsion effect progressively decreases making more favorable the sorption of silver cations onto reactive groups (including amine groups of chitosan and from 2-MBI in addition to sulfur group from 2-MBI). In the case of palladium sorption onto 2-MBI impregnated chitosan, Sharma et al. [57] observed an opposite trend; in that case, the probable predominance of palladium chloroanionic species favors metal binding in acidic solutions. Manohar et al [41] also reported the increase in Hg(II) sorption with pH while using 2-MBI impregnated-clays. Similar trends were observed for Zn(II) sorption on 2-MBI/SBA-15 sorbent [36]. In the case of nano-TiO_2/2-MBI, the sorption was reported to be relatively constant in the range of initial pH 3–9 [54]. For rubidium sorption onto 2-MBI-modified aluminosilicate, the optimum pH was found close to pH 4 [39].

The strong affinity of silver, which is considered a soft metal ions, for the S-reactive groups present at the surface of the sorbent (hold by 2-MBI) may be explained by the Pearson rules (hard and soft acid base theory). Silver ions have a preference for sulfur compounds (soft base) [40].

Fig. S7a shows the pH variation during silver sorption tests: the pH variation increases with the working pH. Below pH 2, the variation is negligible (below 0.5 pH unit). In the range pH 2–4, the pH variation increases up to 1.3 pH unit. From pH 4 to pH 6, the ΔpH tends to decrease. In the range pH 6–7, the pH remains almost unchanged (consistently with pH coming closer to pH_{PZC}). In Fig. S7b, the distribution ratio ($D = q_{eq}/C_{eq}$, L g^{-1}) is plotted in log_{10} unit *vs.* the equilibrium pH. The slope slightly increases with incorporation of magnetite nanoparticles (from 0.060 to 0.078). This slope is frequently associated with proton exchange in mechanisms involving ion-exchange reactions. In the present case, the slopes are not coherent with possible stoichiometric relationship. This is another evidence that the binding mechanism mainly proceeds through chelation mechanisms following preference of silver for sulfur groups. However, some complementary binding mechanisms could involve amine groups (by chelation), especially at the highest pH values. Scheme 2 shows a tentative illustration of sorption mechanisms [37,62].

3.2.2. Uptake kinetics

Among the parameters that can be varied for observing uptake kinetics and identifying the controlling steps in the mass transfer it is possible reporting:

(a) the agitation speed (resistance to film diffusion),
(b) the particle size of the sorbent (intraparticle diffusion),
(c) the concentration of the solute (concentration gradient), or
(d) the temperature (Brownian agitation) [63].

Reducing the size of sorbent particles is expected to accelerate the mass transfer, especially in the case of poorly porous materials. The main drawback of size decreasing consists of the difficult solid/liquid separation at the end of the process. This is precisely the reason for developing magnetic composites for allowing readily magnetic separation of micro/nano particles. Fig. 2a shows that magnetic particles have little lower sorption capacities but the presence of magnetite particles in the sorbent reduces the diffusion path in the particles, which, in turn, reduces the impact of resistance to intraparticle diffusion. This resistance is even more reduced using sonication (especially at high frequency). The combination of magnetic core and sonication allows fast end-separation and strongly enhanced diffusion.

The uptake kinetics have been compared for the two sorbents under different modes of agitation: mechanical agitation (MA) and under ultrasonic treatments using the same power (i.e., 380 W) but with different frequencies: 37 kHz (i.e., UT-F1) and 80 kHz (i.e., UT-F2) (Figs. 2a, 2b and 2c). The sorption processes are usually controlled by different mechanisms, including resistance to diffusion (bulk, film and intraparticle) and the proper reaction rates. Providing a sufficient agitation allows neglecting the resistance to bulk diffusion and minimizing the resistance to film diffusion (or at least limiting its effect to the very first minutes of contact). Testing different types of agitation allows identifying the relative contributions of these modes of resistance to diffusion. Figs. 2a, 2b and 2c clearly demonstrate that sonication considerably increases mass transfer properties. While more than 24 h of contact are necessary for reaching the equilibrium in the case of mechanical agitation (especially for RI sorbent), in the case of sonication 30–40 min are sufficient. Sonication allows introducing cavitation phenomena and acoustic waves that enhance the transfer of solute molecules (both at the surface of the sorbent and in the intraparticle

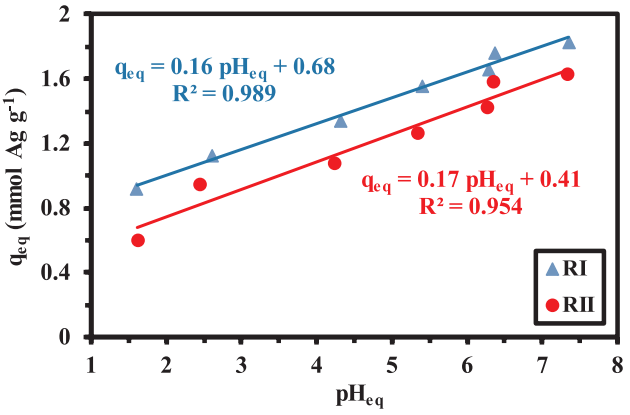

Fig. 1. Effect of pH on Ag(I) sorption using RI and RII sorbents (C_0: 10 mmol Ag L^{-1}; Sorbent Dosage, SD: 1 g L^{-1}; time: 6 h; T; 25 ± 1 °C).

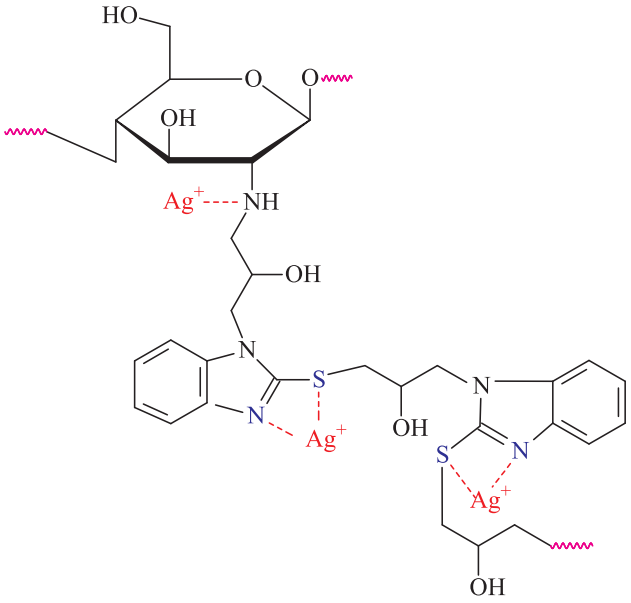

Scheme 2. Suggested mechanisms for Ag(I) sorption on RI.

porous network) and locally affect the internal porosity of the sorbents [43,64–67]. Increasing the frequency, at least within selected frequency range (i.e., 37–80 kHz) improves the sorption of silver: kinetic profiles are systematically shifted to lower residual concentrations at equilibrium. The profiles are parallel: the frequency hardly affects the equilibrium time.

The comparison of RI and RII profiles under mechanical agitation shows that logically the residual concentration is higher for RII sorbent (because of a relatively lower amount of reactive groups in the composite material). However, a pseudo-equilibrium is reached after 4 h of contact (sorption represents 94% of total sorption) while for RI the sorption at 4 h represents only 83% of the sorption achieved after 32 h. The dispersion of magnetite nanoparticles decreases the sorption capacity but contributes to enhance the availability of the reactive groups (despite the decrease in specific surface area). Applying the sonication allows reducing the differences between RI and RII in terms of equilibrium time required for mechanical agitation. Under ultrasonic agitation, the kinetic profiles are parallel.

The figures compare the experimental profiles with fitted curves using the PFORE, the PSORE and the Crank equation (for simplified resistance to intraparticle diffusion, RIDE). The model parameters are summarized in Table 2. The quality of model fitting can be evaluated by three criteria: (a) the comparison of the experimental values of sorption capacity at equilibrium with relevant fitted values, (b) the determination coefficients, and (c) the AIC (Akaike information criterion). In most cases, the PSORE and the RIDE show the best fits of experimental data. The discussion and comparison of theoretical models for fitting kinetic profiles has opened many controversies attached to debatable experimental conditions that in some cases do not allow applying relevant equations (see comprehensive discussion by Simonin [68], Hubbe et al. [69]). In their discussion of literature, Hubbe et al. [69] conclude that frequently the fit of kinetic profiles with the PSORE may be explained by the effective control of mass transfer by the resistance to intraparticle diffusion. It is thus logical finding concomitant good fits for PSORE and RIDE in the current work. The comparison of the parameters for the different systems (RI/RII and MA/UT-F1/UT-F2) shows that the sonication increases the equilibrium sorption capacities compared with mechanical agitation. The ultrasonic treatment increases both the accessibility and the availability of reactive groups. The presence of magnetite nanoparticles (which reduce the fraction of polymer in the composite and then the density of reactive groups) decreases the sorption capacity for mechanical agitation (Δ: −17%), while sonication

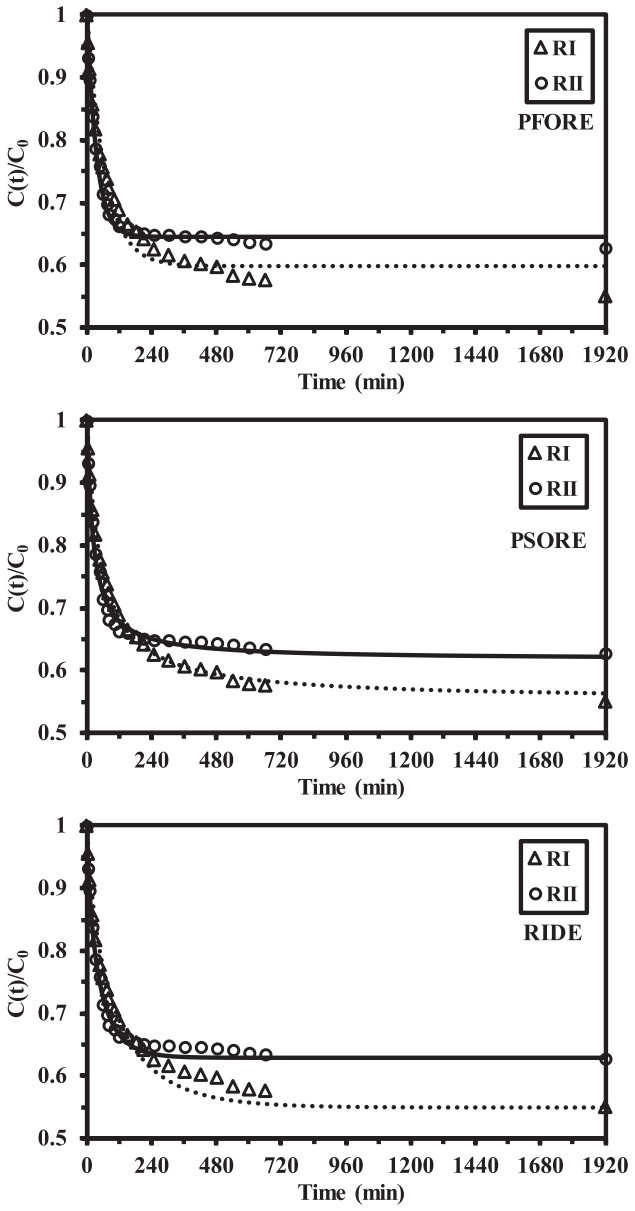

Fig. 2a. Ag(I) uptake kinetics using RI and RII sorbents under MA – Modeling with the PFORE, the PSORE and the RIDE (pH_0: 6.8; C_0: 5 mmol Ag L^{-1}; SD: 1 g L^{-1}; V: 210 rpm; T: 25 ± 1 °C).

enhances sorption capacity (Δ: +17%). The favorable effect of sonication is significantly more marked for RII (Δ: +75–67%) than for RI (Δ: +24–18%). The beneficial effect of sonication is also demonstrated by the comparison of apparent rate coefficients (i.e., k_2). In the range 0.91×10^{-2}-2.31×10^{-2} g $mmol^{-1}$ min^{-1} for mechanical agitation, the rate coefficient increases to 18.4×10^{-2}-16.3×10^{-2} g $mmol^{-1}$ min^{-1} under sonication (at frequency 37 kHz). Increasing more the frequency slightly increases the apparent rate coefficient, up to 24.5×10^{-2}-28.2×10^{-2} g $mmol^{-1}$ min^{-1} at frequency 80 kHz. Increasing the frequency activates the energy transfer associated with the variation of acoustic pressure; the growth and implosion of bubbles formed during the cavitation improve the efficiency of mass transfer [70]. These trends are confirmed by the comparison of the effective diffusivity coefficients (D_e) deduced from RIDE calculations (Crank equation). Under mechanical agitation, the diffusivity coefficient increases from 8.5×10^{-11} m^2 min^{-1} for RI to 30×10^{-11} m^2 min^{-1} for RII. These values are several orders of magnitude lower than self-diffusivity of silver in water (i.e., 9.90×10^{-8} m^2 min^{-1}, [71]).

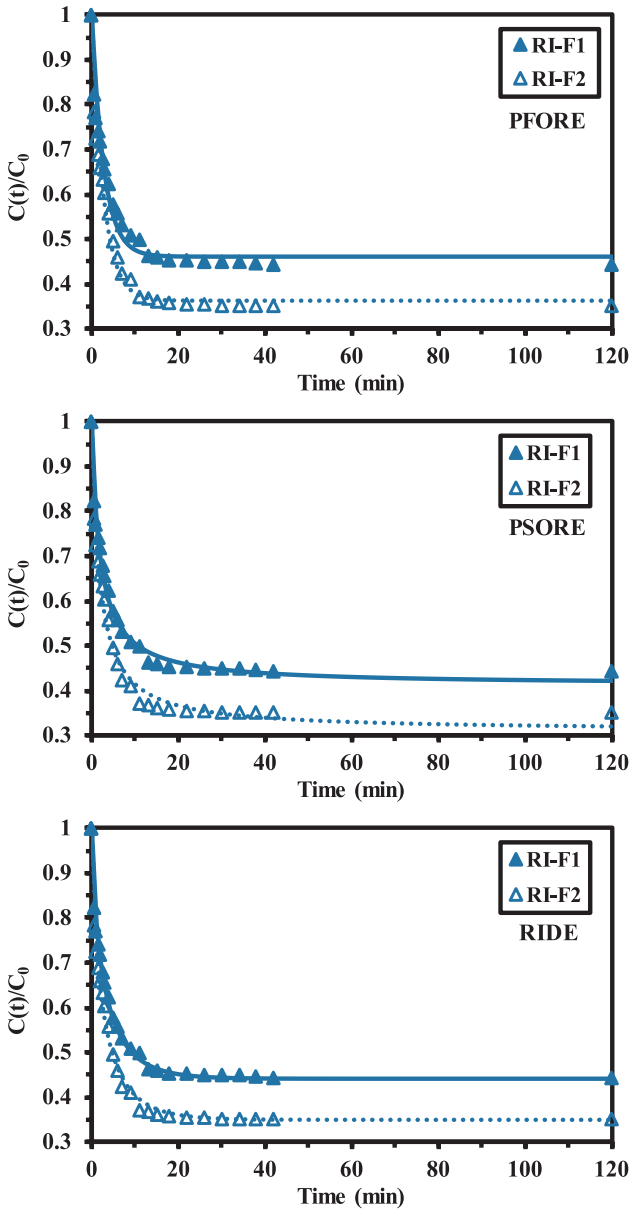

Fig. 2b. Ag(I) uptake kinetics using RI sorbent under ultrasonic treatment with 37 kHz (F1) and 80 kHz (F2) frequencies – Modeling with the PFORE, the PSORE and the RIDE (pH_0: 6.8; C_0: 5 mmol Ag L^{-1}; SD: 1 g L^{-1}; V: 210 rpm; T: 25 ± 1 °C).

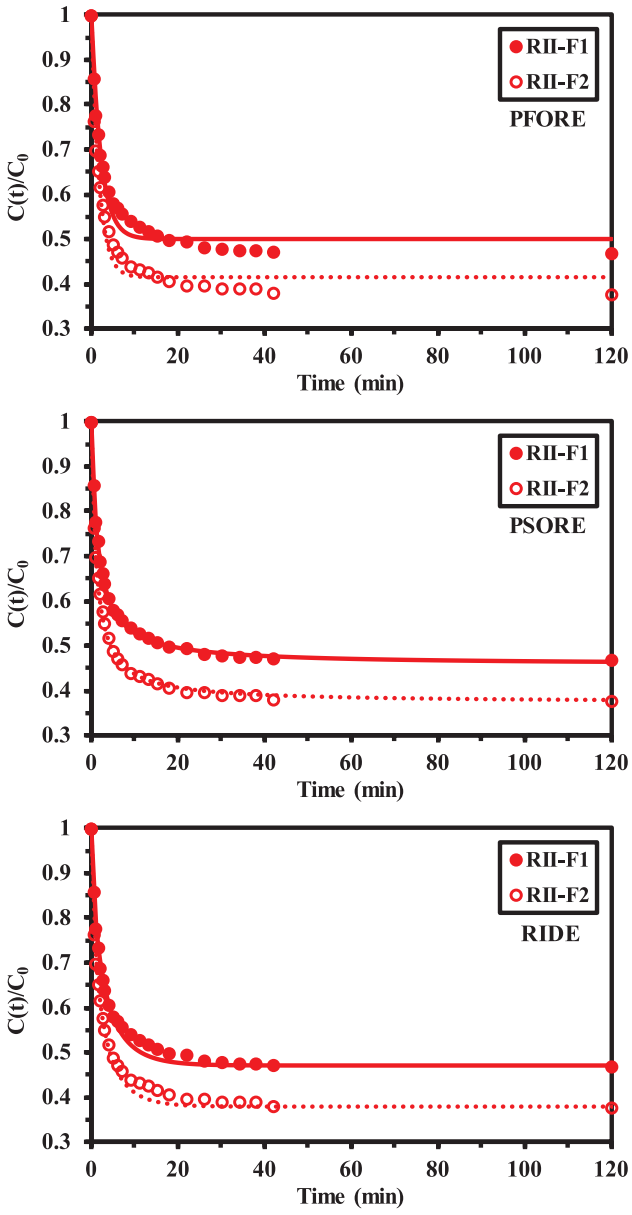

Fig. 2c. Ag(I) uptake kinetics using RI sorbent under ultrasonic treatment with 37 kHz (F1) and 80 kHz (F2) frequencies – Modeling with the PFORE, the PSORE and the RIDE (pH_0: 6.8; C_0: 5 mmol Ag L^{-1}; SD: 1 g L^{-1}; V: 210 rpm; T: 25 ± 1 °C).

Therefore, the resistance to intraparticle diffusion plays a significant role in the control of mass transfer for RI and RII. This resistance can be greatly overcome with ultrasonic treatment. Indeed, the effectivity diffusivity of silver in RI and RII increases to 2.31–2.13 × 10^{-9} m^2 min^{-1} under ultrasonic treatment at the lowest frequency. Increasing the frequency up to 80 kHz improves the mass transfer: the effective diffusivity increases up to 3.61–3.84 × 10^{-9} m^2 min^{-1}. Clearly, sonication limits the resistance to intraparticle diffusion.

3.2.3. Sorption isotherms

The sorption isotherms are reported in Fig. 3 for Ag(I) binding onto RI and RII resins at pH 6.8, and at 25 °C. The figure also compares the profiles for the different modes of agitation. The sorption isotherms are systematically characterized by a saturation plateau (which is reached for relatively high residual metal concentration, in the range 4–5 mmol Ag L^{-1}). The initial slope of the curves, which is correlated to the affinity of the sorbent for the solute, becomes steeper when the

Table 2
Parameters for the modeling of uptake kinetics.

Model	Parameter	MA		UT-F1		UT-F2	
		RI	RII	RI	RII	RI	RII
Exp.	$q_{eq,exp}$ (mmol Ag g^{-1})	2.25	1.86	2.79	3.25	2.65	3.11
PFORE	$q_{eq,1}$ (mmol Ag g^{-1})	2.01	1.77	2.69	3.19	2.50	2.93
	$k_1 \times 10^2$ (min^{-1})	1.50	2.86	35.9	36.8	44.9	55.5
	R^2	0.973	0.994	0.970	0.972	0.972	0.961
	AIC	−169	−211	−157	−151	−166	−153
PSORE	$q_{eq,2}$ (mmol Ag g^{-1})	2.24	1.91	2.93	3.45	2.71	3.14
	$k_2 \times 10^2$ (g $mmol^{-1}$ min^{-1})	0.907	2.31	18.4	16.3	24.5	28.2
	R^2	0.996	0.992	0.980	0.968	0.999	0.991
	AIC	−225	−209	−183	−166	−250	−203
RIDE	$D_e \times 10^9$ (m^2 min^{-1})	0.085	0.30	2.31	2.13	3.61	3.84
	R^2	0.991	0.997	0.988	0.978	0.995	0.991
	AIC	−180	−202	−195	−181	−188	−174

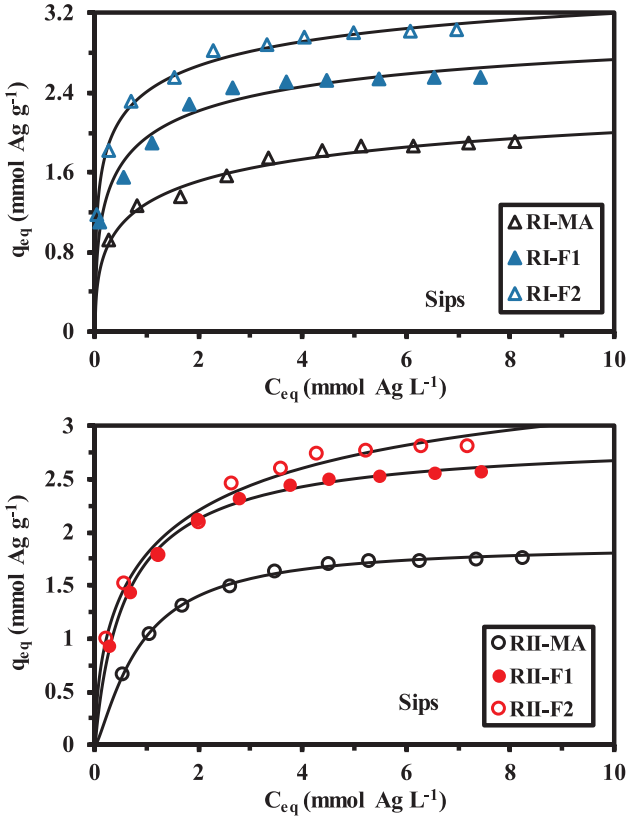

Fig. 3. Ag(I) sorption isotherms at T: 25 °C – Comparison of R1 and R2 sorbents under different agitation modes (MA: mechanical agitation; and ultrasonic treatment with 37 kHz (F1) and 80 kHz (F2) frequencies – Modeling with Sips equation (pH_0: 6.8; C_0: 1.2–10 mmol Ag L^{-1}; SD: 1 g L^{-1}; V: 210 rpm; T: 25 ± 1 °C).

mechanical agitation is replaced with ultrasonic treatment. The benefice is especially important for RI sorbent: the steepness increases with the frequency of the sonication. In the case of magnetic sorbent RII, the effect of the highest frequency of sonication is only detectable for concentrations higher than 2.5 mmol Ag g^{-1}. Different models were tested for fitting experimental profiles: the parameters for the Langmuir, Freundlich, Sips and Temkin equations are summarized in Table 3. The saturation plateau logically disqualifies the Freundlich equation (which supposes an exponential trend). This is confirmed by the values of R^2 and AIC. The Langmuir equation supposes the sorption to occur as a monolayer without interactions between bound molecules, which are sorbed with homogeneous sorption energies at the surface of the sorbent. Another advantage of this model is the relatively good correlation between the experimental and the calculated values at sorbent saturation (monolayer coverage). The Sips equation combines the Langmuir and Freundlich equations; this results in the introduction of a third adjustable parameter. Therefore, the mathematical fit is frequently better, at the expense of a loss in physicochemical significance. The AIC values shows that even taking into account this 3rd-adjustable parameter in the statistical evaluation of the models, the Sips equation is more accurate for fitting experimental data. This model is represented in Fig. 3 by the solid lines. The Temkin equation offers an intermediary quality for mathematical fitting. The model is based on the hypothesis that the adsorption heat decreases with the increase of coverage of sorbent surface with target molecules. While the Langmuir equation covers both physical and chemical sorption, the Temkin equation is frequently associated with chemical sorption. However, Al-Gouthi and Da'ana [72] commented that the use of the Temkin equation is debatable for describing solid/liquid systems (see Fig. 4).

The maximum sorption capacity (i.e., $q_{m,exp}$) is roughly of the same order of magnitude for RI and RII sorbents while the sonication process increases the saturation of the sorbents. This enhancement is even increased at the highest frequency of sonication. The affinity coefficient (i.e., b_L) for Langmuir equation, is systematically lower for RII sorbent compared with RI sorbent (by a factor 2 to 5). The sonication continuously increases the affinity coefficient for RI sorbent (increasing from 2.3 to 4.24 for UT-F1 and up to 9.05 L $mmol^{-1}$ for UT-F2); the enhancement is less marked for RII sorbent from 1.05 to 1.64 L $mmol^{-1}$. The heat of sorption (B_T) slightly decreases with the magnetic core (by 23 to 34%) and by application of ultrasonic agitation (by 15 to 27%). The sonication activates the sorption, which, in turn, requires less energy. The presence of magnetite nanoparticles also decreases the heat of sorption. Calculated against the standard conditions (i.e., RI sorbent under mechanical agitation), the combination of magnetic nanoparticles (i.e., RII sorbent) and sonication decreases sorption heat by 40% at 37 kHz and up to 47% at 80 kHz.

Table 4 summarizes Ag(I) sorption properties for a series of alternative sorbents. Some sorbents have outstanding sorption capacities at saturation that are probably associated with complementary phenomena of precipitation and/or metal reduction [22,73–75]. Indeed, silver is highly sensitive to UV-light irradiation, in addition, some reactive groups such as thiourea have been reported to cause the reduction of silver at the surface of sorbents [21,76]. Except these specific sorbents, the sorption properties of RII (taking into account both the maximum sorption capacity, the equilibrium time but also the regeneration properties and the selectivity criteria, see below) allow ranking this magnetic composite among the most efficient sorbents when sorption is assisted by sonication. The strict comparison of sorption performances is difficult because the influence of complex solutions (and selectivity issues) [22,73], the metal desorption and the sorbent recycling [22] are not systematically investigated. Therefore, RI and RII sorbents demonstrate very attractive properties for sonication-assisted silver sorption due to high sorption capacities, fast kinetics, readily desorption, highly efficient recycling and selectivity (see below).

3.2.4. *Thermodynamics of Ag(I) sorption*

In order to approach more quantitatively the impact of magnetic core and sonication on the thermodynamic characteristics of Ag(I) sorption using 2-MBI/chitosan sorbent (i.e., RI), the sorption isotherms are performed at 4 different temperatures (25–55 °C) (Fig. S8). Systematically, the maximum sorption capacities (corresponding to the saturation plateau) decrease with increasing the temperature. In

Table 3
Parameters for the modeling of sorption isotherms (at 25 °C).

Model	System	MA		UT-F1		UT-F2	
	Sorbent	RI	RII	RI	RII	RI	RII
Experimental	$q_{m,exp}$	1.91	1.77	2.56	2.58	3.04	2.82
Langmuir	$q_{m,L}$	1.96	2.02	2.60	2.81	2.95	3.04
	b_L	2.30	1.05	4.24	1.64	9.05	1.63
	R^2	0.977	0.996	0.958	0.998	0.950	0.979
	AIC	−49	−69	−34	−69	−28	−40
Freundlich	k_F	1.28	1.07	1.88	1.66	2.32	1.76
	n_F	4.77	3.64	5.42	3.93	6.14	3.69
	R^2	0.990	0.960	0.977	0.972	0.989	0.984
	AIC	−58	−43	−41	−39	−45	−43
Sips	$q_{m,S}$	2.87	1.88	3.44	2.90	4.20	4.13
	b_S	0.825	1.21	1.31	1.48	1.36	0.77
	n_S	2.22	0.78	2.15	1.10	2.67	1.75
	R^2	0.994	0.999	0.987	0.999	0.997	0.992
	AIC	−59	−78	−44	−69	−55	−47
Temkin	b_T	7860	6082	6698	4736	6696	4448
	a_T	67.4	13.33	207.5	26.38	753.3	28.41
	R^2	0.993	0.981	0.984	0.990	0.995	0.991
	AIC	−59	−42	−44	−49	−51	−47

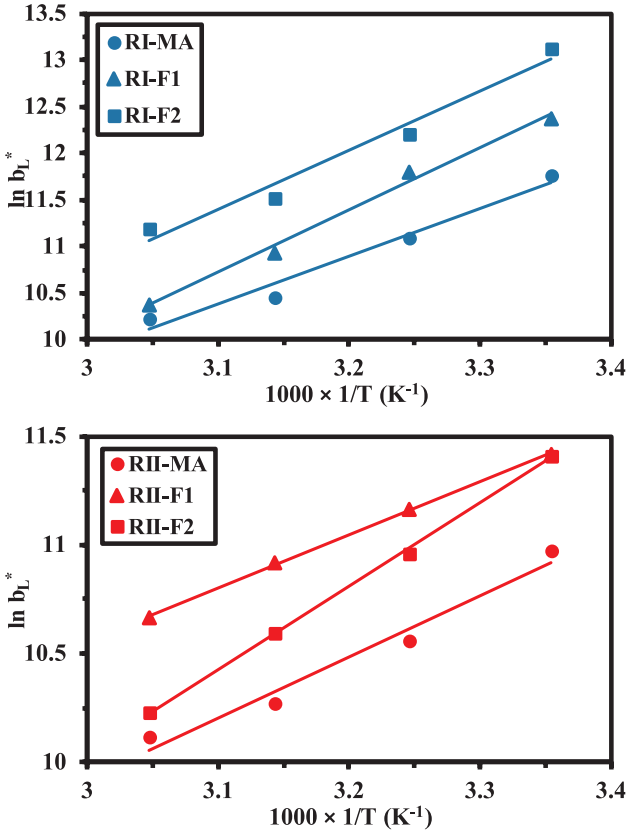

Fig. 4. Van't Hoff plot for the sorption of Ag(I) using RI and RII sorbents under different modes of agitation.

addition, the initial slope of the isotherms, which is correlated to the affinity of the sorbent for silver (and then to b_L), also decreases with increasing the temperature. The sorption of Ag(I) onto RI and RII sorbents is exothermic. The figure shows isotherm profiles together with their fits with the Langmuir equation, which was selected for further applying the van't Hoff equation and calculating the thermodynamic parameters [77]:

$$\ln b_L^* = -\frac{\Delta H^0}{RT} + \frac{\Delta S^0}{R} \quad (3a)$$

$$\Delta G^0 = \Delta H^0 - T\Delta S^0 \quad (3b)$$

where b_L^* is the corrected value of the Langmuir affinity constant (dimensionless parameter $b_L^* = b_L$ (L mol^{-1}) × M_{H2O} (M_{H2O} = 55.51 (mol H_2O L^{-1}), molal concentration of water, [78]); ΔH^0 (kJ mol^{-1}) is the enthalpy change, ΔS^0 (J mol^{-1}K^{-1}) is the entropy change, and ΔG^0 (kJ mol^{-1}) is the Gibbs free energy change.

Table S4 summarizes the parameters for the different systems. The application of the van't Hoff equation allows plotting ln b_L^* *vs.* the reciprocal of absolute temperature and to deduce the thermodynamic parameters collected in Table 5. The negative values of the enthalpy change confirms the exothermic behavior of silver sorption onto 2-MBI/chitosan sorbent. The exothermic character increases with sonication for both RI and RII. For RII, the enthalpy change also continuously increases with the frequency of the sonication process while for RI the enthalpy change tends to slightly decrease at the highest frequency. The entropy change is also systematically negative for RI sorbent: the solid/liquid system is characterized by a lesser activity [77]. The randomness of the system decreases after metal sorption. Surprisingly, for RII sorbent the entropy change is positive for mechanical agitation and sonication at lower frequency while it turns back to negative value for sonication at highest frequency.

The sorption of silver is non-spontaneous (confirmed by the negative value of Gibbs free energy change). Substantial changes are observed between RI and RII: the enthalpy and the entropy changes are substantially lower for RII compared with RI. The magnetic nanoparticles contribute to reduce the impact of temperature, and to enhance the spontaneity of the sorption (lower $|\Delta G^0|$ values). On the other hand, the sonication has a weak impact on the spontaneity of the sorption process for RII sorbent, the non-spontaneity being more significantly increased by sonication for RI sorbent. In the case of RII sorbent, the Gibbs free energy negatively increases with temperature under MA and UT-FI, while its value negatively decreases with temperature for sonication at the highest frequency.

The comparison of the b_T parameters (in the Temkin equation) brings information on the heat of adsorption and the effect of magnetic

Table 4
Ag(I) sorption performances of selected sorbents.

Sorbent	pH_0	Equilibrium time (min)	$q_{m,L}$ (mmol Ag g^{-1})	b_L (L mmol^{-1})	Ref.
Functionalized nano-sorbents	5.7	1800	18.89*	1.24	[74]
Alteromonas sp exopolysaccharides	5.7	~1800	3.09	0.464	[94]
Biogenic Mn Oxide	~4	~600	8.24	1.68	[95]
Superparamagnetic Carbon	n.m.	60	0.57	1.17	[96]
Thiourea-formaldehyde resin	n.m.	7200	22.53	3.09	[22]
Functionalized PAN	6	120	0.53	0.249	[97]
Taurine-cellulose	5.6	1200	0.51	9.92	[76]
Ion-imprinted polymer	6	240	1.09	8.03	[98]
PS/PANI nanobeads	6	1440	2.97	1.83	[73]
Coconut shell activated carbon	3	600	0.74	0.002	[99]
Multi-thiolated cage mesoporous monoliths	6	20	1.67	98.1	[47]
Powdered coffee grounds	6	120	0.37	66.2	[100]
Amazon yeast	4	60	0.45	39.9	[101]
Coconut fiber	4	10	0.77	0.195	[102]
Functionalized MCM48 silica**	5	60	1.38	276	[103]
Functionalized PGMA microbeads	5	840	2.01	7.02	[26]
Dithioxamide polysiloxane	6	2880	5.04	1.37	[24]
nZVI/HPAC	6	40	12.7	1.26	[75]
Functionalized magnetic nanocomposite	5.6	480	7.48	150	[25]
Amino-carbamate alginate beads	5	180	1.95	0.083	[104]
2-MBI chitosan	6.8	1920	1.96	2.30	This work
2-MBI magnetic chitosan	6.8	1920	2.02	1.05	This work
2-MBI chitosan†	6.8	20–30	2.95	9.05	This work
2-MBI magnetic chitosan†	6.8	20–30	3.04	1.63	This work

*Redox effect; ** poor fit with the Langmuir equation; †sonication-assisted sorption; n.m.: not mentioned.

Table 5
Thermodynamics of Ag(I) sorption using RI and RII under different modes of agitation (mechanical agitation, MA; ultrasonic treatment with frequency 37 kHz, UT-F1, and frequency 80 kHz, UT-F2).

Sorbent	Agitation	MA			UT-F1			UT-F2		
	T (°C)	-ΔH°	-ΔS°	-ΔG°	-ΔH°	-ΔS°	-ΔG°	-ΔH°	-ΔS°	-ΔG°
RI	25	42.66	45.89	28.98	55.66	83.43	30.78	52.92	69.33	32.25
	35			28.52			29.95			31.55
	45			28.06			29.11			30.86
	55			27.6			28.28			30.17
RII	25	23.39	−12.33	27.07	20.31	−26.86	28.32	31.87	12.12	28.26
	35			27.19			28.58			28.13
	45			27.31			28.85			28.01
	55			27.44			29.12			27.89

ΔH° and ΔG°, kJ mol^{-1}; ΔS°, J K^{-1} mol^{-1}.

core in relation with sonication (Fig. S9). The lowest heats of adsorption are systematically found positive as a confirmation of the exothermic nature of the sorption process. The lowest values are obtained with sonication at the highest frequency (i.e., UT-F2) and the highest temperature (i.e., 55 °C).

The variations of thermodynamic parameters with incorporation of magnetite nanoparticles and with sonication clearly illustrate the critical effect of these two "parameters" on the design of efficient sorbent and sorption process. This effect can be measured not only in terms of mass transfer but also on equilibrium parameters and thermodynamic criteria (activation of sorption mechanisms).

3.2.5. Metal desorption and sorbent recycling

The desorption of the metal ions from loaded sorbents have a double objective: valorizing the metal (or concentrating hazardous contaminants) and/or recycling the sorbent. Several types of eluents may be used: acidic or alkaline solutions (depending on the impact of pH on sorption performance and mechanisms) or alternatively using metal ligands. In the case of magnetic-based sorbents, the use of strong acid solutions may have a significant impact on the stability of the sorbent (more specifically the partial dissolving of magnetite nanoparticles). In the case of precious metals, it is frequently necessary using a combination of ligand and acid for enhancing metal desorption [23,76,79–81]. Lukinskas et al [82] investigated the complexation of silver with thiourea in acid media. They concluded that, depending on the ratio between silver and thiourea, different complexes may form, based on binuclear complexes (i.e., $Ag_2TU_{n,\ =1\text{-}6}$) (independently of the type of acid and concentration). Silver ions reacts under a four-coordination mode with solvent participation. Silver desorption from metal-loaded RI and RII sorbents was investigated by comparison of the desorption kinetics at different thiourea (TU) concentrations under different modes of agitation (Fig. S10). The TU concentration has a critical effect on the efficiency of the desorption process, especially for systems managed under mechanical agitation. For RI, the concentration of TU must exceed 0.6 M for achieving complete desorption, while RII requires a higher concentration (greater than 0.8 M). The pseudo-equilibrium is reached within 120 min of contact (for MA). When desorption is assisted by sonication the performance of desorption is considerably increased both in terms of effective desorption yield and equilibrium time. The sonication allows reducing the minimum concentration of TU for achieving the complete desorption of silver (> 98%): 0.6 M under UT-F1 and 0.4 M under UT-F2 conditions for both RI and RII. In addition, the contact time required for reaching equilibrium is considerably reduced. For TU concentrations higher than 0.4 M, the equilibrium is reached within 7–10 min for RI and 6–15 min for RII. It is noteworthy that RII sorbent requires stronger conditions for desorption compared with RI sorbent: higher TU concentration and higher sonication frequency. A good compromise for optimized desorption of silver from loaded resins would consist of using 0.8 M TU concentration under sonication at 37 kHz for RI. The benefit at using the higher frequency does not appear clearly. For RII, the sonication should be applied at 80 kHz, with the same TU concentration.

Table 6 summarizes the performances of sorption and desorption for RI and RII along 5 successive cycles of sorption and desorption. The sorption capacity progressively decreases with increasing the number of cycles. However, it is noteworthy than even after 5 cycles, the loss in sorption does not exceed 16% for RI and 13% for RII. The efficiency of desorption remains remarkably stable around 98%. Thiourea is supposed to reduce Cu(II) to Cu(I), Au(III) to Au(I), Pt(IV) to Pt(II) and Te(IV) to Te(II) [83,84]. This reduction may cause some difficulties to desorb the metals and also the progressive saturation of the surface. Apparently, this phenomenon is not observed for Ag(I) on RI and RII sorbents. The saturation of the sorbent nor the poisoning of its surface does not explain the loss in sorption properties. The global desorption properties (with appropriate sonication and optimum selection of TU concentration) offer very promising performances for efficient sorption and sorbent recycling. Metal can then be valorized by electrodeposition from the thiourea eluate [13,85].

Table 6
Sorbent recycling – comparison of sorption and desorption (mmol g^{-1}), desorption efficiencies (individual, $DE_{\#}$, and cumulative, $DE_{cumul.}$, %) for RI and RII on Ag(I) ions for five successive cycles.

Cycle	RI				RII			
	Sorption	Desorption	$DE_{\#}$	$DE_{cumul.}$	Sorption	Desorption	$DE_{\#}$	$DE_{cumul.}$
#1	2.68	2.59	96.6	96.6	2.65	2.59	97.7	97.7
#2	2.56	2.52	98.4	97.5	2.46	2.42	98.4	98.0
#3	2.41	2.35	97.5	97.5	2.41	2.35	97.5	97.9
#4	2.29	2.24	97.8	97.6	2.34	2.32	99.1	98.2
#5	2.25	2.21	98.2	97.7	2.3	2.24	97.4	98.0

Experimental Conditions – Sorption step: SD: 2.5 g L^{-1}; C_0: 5 mM, pH_0: 7.08; contact time: 30 min; T: 298 ± 1 K; ultrasonic agitation: frequency 37 kHz and power 380 W / Desorption using 0.8 M thiourea solution: 20 mL g^{-1} (Ag-loaded sorbent) at pH 2 for RI and pH 4 for RII (pH adjusted using H_2SO_4), t: 30 min under ultrasonic agitation (37 kHz); T: 298 ± 1 K).

3.2.6. Selectivity issues – EDTA effect

The sorption of silver in the presence of equimolar concentration (i.e., 2 mmol L^{-1}) of competitor ions has been investigated for evaluating the selectivity of RI and RII sorbents in acidic solutions. The pH was set to 2 for avoiding metal precipitation and approaching the conditions for the treatment of acidic leachates of E-wastes (Fig. 5a). The same experiments were performed in the presence of EDTA in order to modulate the selectivity of sorption in function of the proper affinity of these competitor ions for the complexing agent (Fig. 5b) [86]. Table S5 reports the main physicochemical characteristics of these metal ions, while Tables S6 and S7 show the distribution of metal species at pH 2 in absence and in presence of EDTA (4 mmol EDTA L^{-1}), respectively.

The selectivity coefficient is calculated as the ratio of silver distribution coefficient against competitor metal ion distribution coefficient:

$$SC_{Ag/Me} = \frac{D_{Ag}}{D_{Me}} = \frac{q_{eq,Ag} \times C_{eq,Me}}{C_{eq,Ag} \times q_{eq,Me}} \quad (4)$$

3.2.6.1. In absence of EDTA. Fig. 5a shows that both RI and RII have a marked preference for Ag(I) against Cu(II), Al(III), Pb(II), Ni(II) and Zn (II): the selectivity coefficient is strictly higher than 8. It is noteworthy that the selectivity is slightly lower for RII compared with RI. For Sn(II), the SC is close to 3. For the other metal ions (i.e., Au(III), Pd(II) and Fe (III)), the sorbents have almost no selectivity for silver: the SC values vary between 0.7 and 1.6; the sorbents cannot be used for separating this series of metals. Table S6 shows that in most cases, under selected experimental conditions, the strongly predominant species (superior to 90%) are the free metal ions (Me^{n+}): gold is essentially present as the hydrolyzed species (i.e., $AuOH^{2+}$, 60.8%) while a non-negligible fraction (about 13%) of Pb(II) exists as nitrate species and about 36% of iron(III) is present as hydrolyzed cationic species. In addition, at pH 2, the sorbents are cationic: amine groups are protonated as well as thiol groups. The selectivity cannot be directly correlated to the speciation of these metal ions. The preference for silver is thus controlled by other criteria such as the Pearson's rules (hard and soft acid base theory) [87]. Table S5 classifies selected metals according their softness/hardness: silver, gold and palladium being soft acids are supposed to show higher affinity in terms of both thermodynamics and kinetics for soft bases. S-based ligands are precisely considered as soft bases. The strong affinity of the sorbents for these metals ions is consistent with HSAB principles; the poor selectivity for Ag(I) *vs.* Au(III) and Pd(II) is also consistent with this analysis. Cu(II), Pb(II), Ni(II) and Zn(II) are borderline metals ions, which are supposed to have a lower affinity for soft bases (such as S-bearing ligands). The sorbents have expectedly high selectivity for Ag(I) against these metal ions and also against Sn(II) (also borderline), though to a lower extent. The behavior of Al(III), hard acid, is also consistent with the good selectivity of the sorbents for Ag(I), in binary solutions. In the case of iron(III), the selectivity coefficients are differing from expected trend: according HSAB theory, Fe(III) is a hard acid, which should have poor affinity for sulfur-based reactive groups. In this specific case, the occurrence of precipitation phenomena due to pH increase during sorption may explain the unexpected increase in the distribution ratio of iron(III). These trends are roughly consistent with the preferential affinity of 2-MBI for silver against Cu(II) < Fe(III)/Pb(II) and Zn(II) [37], or the comparable sorption properties of 2-MBI grafted on silica-gel for Cu(II), Zn(II and Pb(II) at pH 3–5 [88].

Fig. S11a-b compares the sorption capacities for Ag(I) and co-metal from binary solutions for both RI and RII. For RI, Ag(I) sorption capacities decrease according: Pb(II) > Ni(II) ≈ Al(III) ≈ Zn(II) > Cu (II) > Sn(II) > Fe(III) > Au(III) > Pd(II),

While competitor metal sorption capacities can be ranked according:

Pd(II) > Fe(III) > Au(III) > Sn(II) > Ni(II) > Zn(II) ≈ Pb (II) ≈ Al(III) ≈ Cu(II).

The cumulative sorption capacities range between 1 and 1.25 mmol metal g^{-1}. These values are of the same order of magnitude than the sorption capacity reached in Fig. 1 (study of pH effect). The sorption capacity was close to 1.13 mmol Ag g^{-1} for a metal concentration C_0 close to 5 mmol. For RII resin, the different ranking are reported below, first for Ag(I) sorption capacity in the presence of competitor metals:

Pb(II) > Ni(II) > Zn(II) > Cu(II) ≈ Al(III) > Sn(II) > Fe (III) ≈ Pd(II) > Au(III),

and for competitor metal ion:

Fe(III) ≈ Au(III) > Pd(II) > Sn(II) > Zn(II) > Ni(II) > Pb (II) > Cu(II) > Al(III).

The cumulative sorption capacity varies between 0.9 and 1.24 mmol metal g^{-1}; this is comparable to the sorption capacity for Ag(I) at pH_0: 2 (i.e., mono-component solution with C_0: 5 mmol Ag L^{-1}).

3.2.6.2. In presence of EDTA. Ethylenediamine tetraacetic acid is frequently used as a masking agent for the separation of metal ions in solvent extraction [86], or sorption processes [89–92]. The sorption properties of the series investigated in the preceding section were compared with the recovery performances in the presence of EDTA (at the concentration of 4 mmol EDTA L^{-1}). Table S7 shows the effect of EDTA on the speciation of metal ions in binary solutions by comparison with Table S6. The stability constants for Ag(I) are much lower than for the other base metals. Therefore, EDTA binds preferentially other metal cations and silver remains under its free Ag^+ form (98.5%, silver nitrate constituting the residual silver fraction). Gold is not reported to be chelated with EDTA; actually, the chelating agent was used for controlled reduction (depending on the pH) for the preparation of gold nanoparticles [93]. The distribution of gold between Au^{3+} and $AuOH^{2+}$ species is hardly changed. For the other metals, the presence

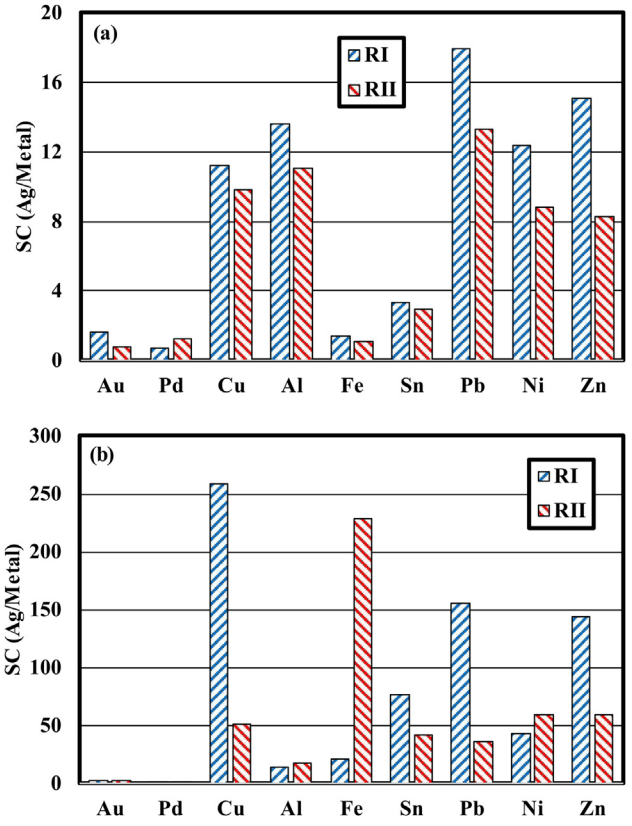

Fig. 5. Selectivity coefficient for the separation of Ag(I) from selected metal ions in binary solutions using RI and RII sorbents: (a) water solution, and (b) in the presence of 0.04 M EDTA (pH_0: 2; C_0: 2 mmol metal L^{-1}; SD: 1 g L^{-1}; Time: 30 min; T: 25 ± 1 °C; ultrasonic treatment with frequency: 37 kHz, UT-F1).

of EDTA strongly changes metal speciation with formation of predominant complexes:

$PdEDTA^{2-}$ (100%),

$CuH_xEDTA^{(2-x)-}$ (with x = 0–2, 100%, 43.4% of anionic species and 56.6% neutral species), $AlH_xEDTA^{(1-x)-}$ (with x = 0–1, 97.7%, 14.9% of anionic species and 82.8% neutral species),

$FeH_xEDTA^{(1-x)-}$ (with x = 0–1, 100%, 78.6% of anionic species and 21.4% neutral species),

$SnH_xEDTA^{(2-x)-}$ (with x = 0–2, 99.9%, 79.0% of anionic species and 25.9% neutral species),

$PbH_xEDTA^{(2-x)-}$ (with x = 0–3, 99.9%, 60.9% of anionic species, 32.8% neutral species and 6.2% cationic species),

$NiH_xEDTA^{(2-x)-}$ (with x = 0–2, 100%, 90.8% of anionic species and 9.2% neutral species),

$ZnH_xEDTA^{(2-x)-}$ (with x = 0–2, 98.1%, 81.8% of anionic species and 16.3% neutral species),

On the other side, the speciation of EDTA-based species and complexes show the coexistence of anionic, neutral and cationic species. In acidic solutions, protonated amine and thiol groups may bind anionic species (both metal complexes and chelating agent species) by electrostatic attraction and neutral or cationic species by chelation. Fig. 5b shows the values of $SC_{Ag/Me}$ for the different binary solutions. For RI, the presence of EDTA allows reaching very high selectivity for Ag(I) over Cu(II) (259) > Pb(II) (156) > Zn(II) (144) > Sn(II) (77) > Ni (II) (43) > Fe(III) (21) > Al(III) (15). On the opposite hand, the SC values are much lower for Au(III) (2.3) > Pd(II) (1.0). The chelation of base metals with EDTA decreases their availability for binding on 2-MBI groups. In the case of RII, the sorbent has also a marked preference for Ag(I) over base metals but the selectivity coefficients are much lower than the values reported for RI sorbent, except for Fe(III) where the $SC_{Ag/Fe}$ increases up to 229 (*vs.* 21.4 for RI), and Al(III) (17.5 *vs.* 14.6 for RI). For Au(III) and Pd(II), the SC values are of the same order for both RI and RII sorbents (2.2 and 1.16, respectively). Gold sorption is not affected by EDTA and the good affinity of soft sulfur groups for soft acids such as Ag(I) and Au(III) explains the good simultaneous sorption of the two metal ions. On the other hand, palladium appears to be completely complexed by EDTA to form a divalent anion ($PdEDTA^{2-}$). Despite this change in metal speciation, the sorption of Pd(II) remains quite favorable. The sorption capacities for Pd(II) (0.59 and 0.47 mmol Pd g^{-1} for RI and RII, respectively) are close to the relevant values for Ag(I) (0.57 and 0.51 mmol Ag g^{-1}, respectively) (Fig. S11c-d). The sorption capacities for base metals are significantly decreased in the presence of EDTA. It is noteworthy that the cumulative sorption capacities remain of the same order than the values reached in the absence of EDTA (in the range 1.08–1.32 mmol g^{-1} for RI and 0.91–1.21 mmol g^{-1}). Silver contribution in the total sorption capacity obviously increases against base metals in the presence of EDTA.

Fig. S12 summarizes the positive/negative effects of EDTA on Ag(I) and competitor metal ions in binary solutions for RI and RII sorbents by comparison of sorption capacities (Δq_{eq}) for the different couples of metal ions in presence and absence of the ligand. For RI, the addition of EDTA increases Ag(I) sorption capacities according:

Fe(III) (56%) > Sn(II) (30%) > Cu(II) (23%) > Pd(II) (21%) > Au(III) (19%) > Ni(II) (18%) > Zn(II) (14%) > Al(III) (7%).

The ligand drastically decreases the sorption of base metals (in the range 56–93%); the variations are rather limited for the binding of Au (III) and Pd(II) (loss in sorption capacity lower than 8%), while the binding of Al(III) slightly increases (by less than 7%).

Similar trends (with different amplitudes) are observed for RII sorbent (Fig. S12b). The main difference with RI are associated with Pd(II) (weak loss for Ag(I) binding), for Al(III) (higher increase of Ag(I) sorption) and Fe(III) (iron is not sorbed while silver sorption capacity is doubled).

EDTA plays an important role in the masking of base metals for limiting their sorption and making more sites available for the binding of precious metals at pH 2. The selectivity for Ag(I) against base metals is significantly enhanced while using EDTA. The effect is negligible when considering precious metals (weak acids with high affinity for sulfur-reactive groups of 2-MBI) because of their weak binding to EDTA (whose functional groups can be classified as hard base).

Table 7
Composition of acidic leachate of E-waste and concentration factor (CF, after resin elution).

Metal	C_0 (mg L^{-1})	C_0 (μmol $L^{-1)}$	CF
Ag	1.46	13.6	46.7
Au	0.25	1.3	46.9
Pd	0.23	2.2	41.6
Cu	135.46	2132	0.02
Al	48.34	1792	0.35
Fe	45.52	815.0	0.07
Sn	23.73	199.9	0.47
Pb	16.91	81.6	0.17
Ni	9.84	167.7	1.12
Zn	8.32	127.2	1.15

3.2.7. Application to ore leachate

The composition of the acidic leachate (pH 2) is summarized on Table 7. The concentration of base metals (BMs) is in large excess compared with the concentration of precious metals (PMs): the conditions are relatively unfavorable for silver valorization. The leachate contains 17.1 μmol L^{-1} of PMs (79.5% as Ag) and 5315 μmol L^{-1} of BMs (including: Cu(II) 40%, Al(III) 34% and Fe(III) 1%).

Fig. 6a shows the high sorption efficiency of RI for PMs (at low concentrations): the sorption efficiency varies between 85% and 98% (for Ag(I)) while for BMs the sorption efficiencies are lower than 3%. Residual metal concentrations are lower than 0.32 μmol L^{-1} for PMs, showing the effectiveness of the sorbent for exhausting the solution. On the opposite hand, the residual concentrations are very high for BMs: the sorbent is relatively selective to PMs; consistently with the trends observed in the preceding section.

Fig. 6b shows the enrichment factor (EF = molar fraction in the sorbent/molar fraction in the leachate) for the different metals. The sorption steps on RI allow substantially enriching the fraction of PMs' traces (in the range 114–130) while for BM majors the EF never exceeds 3.2. The sorption capacity for silver reaches 13.3 μmol Ag g^{-1} (despite the very low concentration in the leachate); this is much higher than the values reached for other PMs (1.22–1.86 μmol g^{-1}) and BMs (lower than 3.8 μmol g^{-1}). The figure also shows that desorption efficiencies systematically exceed 95%. This is consistent with the results obtained at

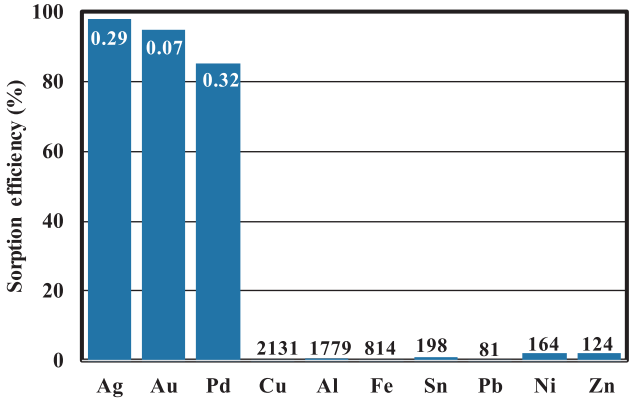

Fig. 6a. Testing of RI sorbent for the treatment of leachate of E-waste - Sorption efficiency (%), Numbers: Residual metal concentration, μmol L^{-1} (Sorption pH_0: 1.95; pH_{eq}: 2.76; SD: 1 g L^{-1}; 25 ± 1 °C; Time: 15 min; Agitation mode: UT-F1, 37 kHz frequency – Desorption (SD: 1 g sorbent/20 mL eluent; T: 25 ± 1 °C ; contact time: 10 min; Agitation mode: UT-F1).

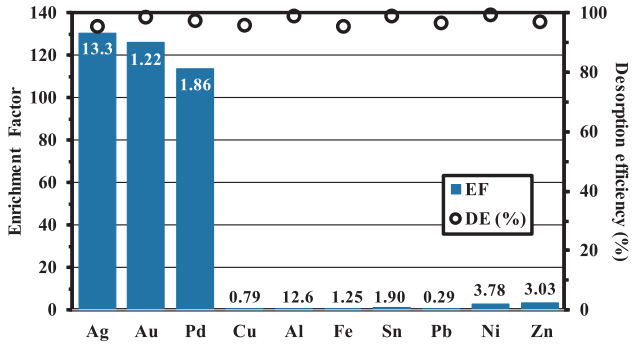

Fig. 6b. Testing of RI sorbent for the treatment of leachate of E-waste - Enrichment Factor, EF: molar proportion on the sorbent/molar proportion in the leachate; desorption efficiency, DE (○), Numbers: metal sorption capacity, μmol g^{-1} (Sorption pH_0: 1.95; pH_{eq}: 2.76; SD: 1 g L^{-1}; 25 ± 1 °C; Time: 15 min; Agitation mode: UT-F1, 37 kHz frequency – Desorption (SD: 1 g sorbent/20 mL eluent; T: 25 ± 1 °C ; contact time: 10 min; Agitation mode: UT-F1).

least for Ag(I) at Section 3.2.5. The sorbent metals can then be recovered and valorized and the sorbent can be recycled. These results demonstrate the high potential of this material for recovering silver (and other PMs) even at low metal concentration from very complex solutions containing a large collection of base metals (in large molar excess, ~67 times).

Table 7 also reports the concentration factor (CF) defined as the concentration of the metal in the eluate of the resin and its concentration in the leachate. Precious metals are strongly concentrated in the eluate: the CF ranges between 41 and 47. Nickel and zinc are found in the eluate at approximately the same concentration as in the leachate: CF varies between 1.12 and 1.16. For the other metals, the selectivity of Resin RI is confirmed by the depletion of their concentrations in the eluate: the CF ranges between 0.02 and 0.47.

4. Conclusion

The functionalization of chitosan with 2-mercaptobenzimidazole brings to the biopolymer high affinity for silver (and other precious metals). Soft acids are efficiently bound to soft bases as sulfur-based reactive groups. This may explain the high selectivity of the sorbent for precious metals against base metals. The selectivity can be enhanced using EDTA as a masking agent (binding of base metals to EDTA; the complexes becoming less available for binding on 2-MBI moieties.

More specifically to Ag(I), sorption increases with pH. Uptake kinetics is relatively slow: under selected experimental conditions, 24–28 h are necessary for reaching equilibrium. This is probably due to the low specific surface area. The incorporation of magnetic nanoparticles weakly improves mass transfer properties (independently of the loss of specific surface area). However, the resistance to intraparticle diffusion can be readily overcome using sonication for assisting metal sorption: 20–30 min are sufficient for reaching equilibrium under the same experimental conditions. The sorption capacities increase compared with mechanical agitation and the effective diffusivity of Ag(I) in the sorbents significantly increases with sonication (especially at the highest frequency: 80 kHz *vs.* 37 kHz). The maximum sorption capacities are thus affected by the incorporation of magnetic nanoparticles (relative decrease of reactive groups by substitution of magnetite NPs) and the type of agitation (MA *vs.* UT-F1 and UT-F2). The maximum sorption capacity (up to 3.04 mmol Ag g^{-1}) is reached for non-magnetic sorbent with sonication at the higher frequency. The sonication activates the sorbent for enhanced sorption not only in terms of kinetics but also under thermodynamic criteria. The sorption of silver is exothermic, non-spontaneous and operates with decrease in the randomness of the system (as shown by the sorption isotherms obtained in the range 25–55 °C). The sorption isotherms are fitted by the Langmuir equation.

Metal desorption is highly efficient with acid solutions of thiourea (controlling the pH at 2 for RI and 4 for RII, to avoid possible degradation of magnetite NPs in excessively acid solutions). Applying sonication allows reducing the concentration of thiourea to be used for achieving the complete desorption of silver and for speeding up the release of silver. Desorption is highly efficient (greater than 98%) and stable along a minimum of 5 cycles, while sorption slightly decreases with recycling (about 13–16% at the fifth cycle).

This work clearly demonstrates the interest of cavitation effect induced by sonication for the improvement of sorption and desorption properties. This beneficial effect is appearing more clearly than the proper effect of the incorporation of magnetite nanoparticles.

Applied to the treatment of an acidic leachate of printed circuit cardboard, the sorbent RI shows outstanding preferences for precious metals against base metals (despite the much lower concentration levels of PMs compared with BMs). This is clearly demonstrated by the gap observed in terms of selectivity coefficients, enrichment and concentration factors between PMs and BMs.

The combination of chitosan functionalization with 2-MBI and the sonication treatment allows designing a very efficient process for the recovery of precious metals from acidic leachates.

CRediT authorship contribution statement

Khalid Z. Elwakeel: Conceptualization, Methodology, Data curation, Investigation. **Abdullah S. Al-Bogami:** Funding acquisition, Methodology, Investigation, Validation. **Eric Guibal:** Conceptualization, Writing - review & editing.

Declaration of Competing Interest

The authors declare that they have no known competing financial interests or personal relationships that could have appeared to influence the work reported in this paper.

Acknowledgements

This work was funded by the University of Jeddah, Saudi Arabia, under grant No. UJ-39-18-DR. The authors, therefore, acknowledge with thanks the university's technical and financial support. EG acknowledges the support of Institut Français d'Egypte for structuring the collaboration network between IMT – Mines Ales and Egyptian institutions (including Port Said University).

Appendix A. Supplementary data

Supplementary data to this article can be found online at https://doi.org/10.1016/j.cej.2020.126265.

References

[1] K. Habib, K. Parajuly, H. Wenzel, Tracking the flow of resources in electronic waste – the case of end-of-life computer hard disk drives, Environ. Sci. Technol. 49 (2015) 12441–12449.
[2] V. Innocenzi, I. De Michelis, B. Kopacek, F. Veglio, Yttrium recovery from primary and secondary sources: a review of main hydrometallurgical processes, Waste Manage. (Oxford) 34 (2014) 1237–1250.
[3] European Commission, Waste Electrical & Electronic Equipment (WEEE) – http://ec.europa.eu/environment/waste/strategy.htm, http://ec.europa.eu/environment/waste/strategy.htm, Accessed: 1/9/2017.
[4] P. Jadhao, G. Chauhan, K.K. Pant, K.D.P. Nigam, Greener approach for the extraction of copper metal from electronic waste, Waste Manage. (Oxford) 57 (2016) 102–112.
[5] M. Sethurajan, E.D. van Hullebusch, D. Fontana, A. Akcil, H. Deveci, B. Batinic, J.P. Leal, T.A. Gasche, M.A. Kucuker, K. Kuchta, et al., Recent advances on hydrometallurgical recovery of critical and precious elements from end of life electronic wastes-a review, Crit. Rev. Env. Sci. Technol. 49 (2019) 212–275.

[6] V. Savvilotidou, E. Gidarakos, Pre-concentration and recovery of silver and indium from crystalline silicon and copper indium selenide photovoltaic panels, J. Cleaner Prod., 250 (2020) Art. N° 119440.
[7] W. Guo, S. Zhang, N. Zhu, D. Luo, P. Wu, Recovery of high purity secondary silver from waste Ag/Cu electrical contacts, Process Saf. Environ. Prot. 127 (2019) 197–205.
[8] N.R. Rodriguez, B. Onghena, K. Binnemans, Recovery of lead and silver from zinc leaching residue using methanesulfonic acid, ACS Sustainable Chem. Eng. 7 (2019) 19807–19815.
[9] W.D. Xing, M.S. Lee, G. Senanayake, Recovery of metals from chloride leach solutions of anode slimes by solvent extraction. Part II: Recovery of silver and copper with LIX 63 and Alamine 336, Hydrometallurgy, 180 (2018) 49-57.
[10] S.-Y. Cho, W.-G. Lee, P.-P. Sun, Solvent extraction separation of silver(I) and zinc (II) from nitrate leach solution of spent silver oxide batteries with D2EHPA, Mater. Trans., JIM 60 (2019) 1090–1095.
[11] N.A. Grigorieva, I.Y. Fleitlikh, N.I. Pavlenko, O.A. Logutenko, Silver extraction from nitrate solutions with the disulfide of bis(2,4,4-trimethylpentyl)dithiophosphinic acid, Hydrometallurgy, 189 (2019) Art. N° 105108.
[12] S.-Y. Cho, T.-Y. Kim, P.-P. Sun, Recovery of silver from leachate of silicon solar cells by solvent extraction with TOPO, Sep. Purif. Technol. 215 (2019) 516–520.
[13] T. Nawaz, S. Sengupta, C.-L. Yang, Silver recovery as Ag-0 nanoparticles from ion-exchange regenerant solution using electrolysis, J. Environ. Sci. 78 (2019) 161–173.
[14] Z. Wang, P. Halli, P. Hannula, F. Liu, B.P. Wilson, K. Yliniemi, M. Lundstrom, Recovery of silver from dilute effluents via electrodeposition and redox replacement, J. Electrochem. Soc. 166 (2019) E266–E274.
[15] A. Musina, S. van Zutphen, V. Lavric, Late transition metal recovery from a silver nitrate electrolyte using a phosphine-oxide bearing scavenger, New J. Chem. 42 (2018) 7969–7975.
[16] M. Chanda, S.A. Pillay, A. Sarkar, J.M. Modalk, A novel fiber-coated strong base-type anion exchanger with superfast kinetics. Removal and recovery of silver thiosulfate from aqueous solutions, J. Appl. Polym. Sci. 100 (2006) 2604–2613.
[17] D. Villemin, C. Monteil, N. Bar, M.A. Didi, Phosphonated polyethyleneimines (PEIP) as multi-use polymers, Phosphorus Sulfur Rel. Elem. 190 (2014) 879–890.
[18] M. Pilsniak-Rabiega, K. Wejman, J. Wolska, Novel conventional and chelating anion exchange resins with amino ligands for sorption of silver, Sep. Sci. Technol., (2019) Art. N° 1639741.
[19] S. Kirci, M. Guelfen, A.O. Aydin, Separation and recovery of silver(I) ions from base metal ions by thiourea- or urea-formaldehyde chelating resin, Sep. Sci. Technol. 44 (2009) 1869–1883.
[20] X. Huang, X. Cao, W. Wang, H. Zhong, Z.-F. Cao, Investigation of removal of Ag(I) from aqueous solution by a novel chelating resin containing acyl and thiourea groups, J. Dispersion Sci. Technol. 40 (2019) 477–486.
[21] P. Kumar, K.B. Ansari, A.C. Koli, V.G. Gaikar, Sorption behavior of thiourea-grafted polymeric resin toward silver ion, reduction to silver nanoparticles, and their antibacterial properties, Ind. Eng. Chem. Res. 52 (2013) 6438–6445.
[22] Z. Hao, Y. Guo, P. Wu, M. Mansuer, J. Zhu, Adsorption properties of silver ions on thiourea-formaldehyde resin, in: W. Pan, Q.J. Xu, H. Li (Eds.) Exploration and Processing of Mineral Resources, 2014, pp. 459-462.
[23] J.-I. Yun, S. Bhattarai, Y.-S. Yun, Y.-S. Lee, Synthesis of thiourea-immobilized polystyrene nanoparticles and their sorption behavior with respect to silver ions in aqueous phase, J. Hazard. Mater. 344 (2018) 398–407.
[24] L.K. Neudachina, A.S. Kholmogorova, I.S. Puzyrev, Z.R. Galieva, Exchange capacity of polysiloxane ion exchangers modified with dithiooxamide groups with respect to silver(I), platinum(IV), and palladium(II), Russ. J. Phys. Chem. A 92 (2018) 2309–2314.
[25] T. Mahlangu, R. Das, L.K. Abia, M. Onyango, S.S. Ray, A. Maity, Thiol-modified magnetic polypyrrole nanocomposite: An effective adsorbent for the adsorption of silver ions from aqueous solution and subsequent water disinfection by silver-laden nanocomposite, Chem. Eng. J. 360 (2019) 423–434.
[26] C. Xiong, S. Wang, L. Zhang, Y. Li, Y. Zhou, J. Peng, Selective recovery of silver from aqueous solutions by poly (glycidyl methacrylate) microsphere modified with trithiocyanuric acid, J. Mol. Liq. 254 (2018) 340–348.
[27] A.M. Donia, A.A. Atia, K.Z. Elwakeel, Recovery of gold(III) and silver(I) on a chemically modified chitosan with magnetic properties, Hydrometallurgy 87 (2007) 197–206.
[28] M. Hosoba, K. Oshita, R.K. Katarina, T. Takayanagi, M. Oshima, S. Motomizu, Synthesis of novel chitosan resin possessing histidine moiety and its application to the determination of trace silver by ICP-AES coupled with triplet automated-pretreatment system, Anal. Chim. Acta 639 (2009) 51–56.
[29] B. Pascu, C. Ardean, C.M. Davidescu, A. Negrea, M. Ciopec, N. Duteanu, P. Negrea, G. Rusu, Modified chitosan for silver recovery-kinetics, Thermodynamic, and equilibrium studies, Materials, 13 (2020) Art. N° 13030657.
[30] Y.S. Petrova, A.V. Pestov, L.M.K. Alifkhanova, L.K. Neudachina, Effect of the degree of cross-linking of N-2-sulfoethylchitosan on the sorption selectivity of copper (II) and silver(I), Russ. J. Appl. Chem. 88 (2015) 1434–1439.
[31] Y.S. Petrova, A.V. Pestov, L.M.K. Alifkhanova, L.K. Neudachina, Dynamics of the sorption of sopper(II) and silver(I) by materials based on sulfoethylchitosan with various degrees of crosslinking, Russ. J. Phys. Chem. A 91 (2017) 766–770.
[32] K.Z. Elwakeel, A.A. Atia, Uptake of U(VI) from aqueous media by magnetic Schiff's base chitosan composite, J. Cleaner Prod. 70 (2014) 292–302.
[33] M.F. Hamza, J.-C. Roux, E. Guibal, Uranium and europium sorption on amidoxime-functionalized magnetic chitosan micro-particles, Chem. Eng. J. 344 (2018) 124–137.
[34] O.V. Kharissova, H.V.R. Dias, B.I. Kharisov, Magnetic adsorbents based on micro- and nano-structured materials, RSC Adv. 5 (2015) 6695–6719.
[35] A. Parodi, T. Vincent, M. Pilsniak, A.W. Trochimczuk, E. Guibal, Palladium and platinum binding on an imidazol containing resin, Hydrometallurgy 92 (2008) 1–10.
[36] B. Sreenu, N. Sathish Kumar, N. Seshadri, K. Seshaiah, A.P. Singh, Synthesis and characterization of 2-mercaptobenzimidazole mesoporous silica SBA-15 and its application in removal of Zn(II) from aqueous solution, Sci. Spectr. 1 (2016) 428–438.
[37] W. Qin, J. Wang, S. Xu, Q. Xie, Z. Xu, Selectivity of 2-mercaptobenzimidazole derivatives on metal ions studied by UV–vis spectromentry and DFT calculations, Colloids Surf., A 490 (2016) 318–325.
[38] O. Mahmoudi, T. Bordjiba, A.M. Affoune, Density functional theory study of the interaction of 2-mercaptobenzimidazole and gold, palladium and nickel atoms, Int. J. Electrochem. Sci. 11 (2016) 4427–4441.
[39] D.L. Guerra, A.C. Batista, R.R. Viana, C. Airoldi, Adsorption of rubidium on raw and MTZ- and MBI-imogolite hybrid surfaces: An evidence of the chelate effect, Desalination 275 (2011) 107–117.
[40] T.S. Anirudhan, P.S. Suchithra, L. Divya, Adsorptive potential of 2-mercapto-benzimidazole-immobilized organophilic hydrotalcite for mercury(II) ions from aqueous phase and its kinetic and equilibrium profiles, Water Air Soil Pollut. 196 (2009) 127–139.
[41] D.M. Manohar, K.A. Krishnan, T.S. Anirudhan, Removal of mercury(II) from aqueous solutions and chlor-alkali industry wastewater using 2-mercaptobenzimidazole-clay, Water Res. 36 (2002) 1609–1619.
[42] Z. Wen, K. Huang, Y. Niu, Y. Yao, S. Wang, Z. Cao, H. Zhong, Kinetic study of ultrasonic-assisted uranium adsorption by anion exchange resin, Colloids Surf., A, 585 (2020) Art. N° 124021.
[43] M. Sheydaei, A.B. Gasemsoltanlu, A. Beiraghi, Optimization of ultrasonic-assisted copper ion removal from polluted water by a natural clinoptilolite nanostructure through a central composite design, Clay Minerals 54 (2019) 339–347.
[44] K.Z. Elwakeel, A. Shahat, Z.A. Khan, W. Alshitari, E. Guibal, Magnetic metal oxide-organic framework material for ultrasonic-assisted sorption of titan yellow and rose bengal from aqueous solutions, Chem. Eng. J., 392 (2020) Art. N° 123635.
[45] K.Z. Elwakeel, A. Shahat, A.S. Al-Bogami, B. Wijesiri, A. Goonetilleke, The synergistic effect of ultrasound power and magnetite incorporation on the sorption/desorption behavior of Cr(VI) and As(V) oxoanions in an aqueous system, J. Colloid Interface Sci. 569 (2020) 76–88.
[46] R. Massart, Preparation of aqueous magnetic liquids in alkaline and acidic media, IEEE Trans. Magn. 17 (1981) 1247–1249.
[47] E.A. Elshehy, M.A. Shenashen, M.O.A. El-Magied, D.A. Tolan, A.M. El-Nahas, K. Halada, A.A. Atia, S.A. El-Safty, Selective recovery of silver(I) ions from E-waste using cubically multithiolated cage mesoporous monoliths, Eur. J. Inorg. Chem. 4823–4833 (2017).
[48] B. Tanhaei, A. Ayati, M. Lahtinen, M. Sillanpää, Preparation and characterization of a novel chitosan/Al2O3/magnetite nanoparticles composite adsorbent for kinetic, thermodynamic and isotherm studies of Methyl Orange adsorption, Chem. Eng. J. 259 (2015) 1–10.
[49] S.M. Hosseini, H. Younesi, N. Bahramifar, Z. Mehraban, A novel facile synthesis of the amine-functionalized magnetic core coated carboxylated nanochitosan shells as an amphoteric nanobiosupport, Carbohydr. Polym. 221 (2019) 174–185.
[50] J.-B. Qu, H.-H. Shao, G.-L. Jing, F. Huang, PEG-chitosan-coated iron oxide nanoparticles with high saturated magnetization as carriers of 10-hydroxycamptothecin: preparation, characterization and cytotoxicity studies, Colloids Surf., B 102 (2012) 37–44.
[51] S. Yu, J. Wang, J. Cui, Preparation of a novel chitosan-based magnetic adsorbent CTS@SnO_2@Fe_3O_4 for effective treatment of dye wastewater, Int. J. Biol. Macromol. 156 (2020) 1474–1482.
[52] W.O. Foye, J.-R. Lo, Metal-binding abilities of antibacterial heterocyclic thiones, J. Pharm. Sci. 61 (1972) 1209–1212.
[53] G. Jerez, G. Kaufman, M. Prystai, S. Schenkeveld, K. Donkor, Determination of thermodynamic pKa values of benzimidazole and benzimidazole derivatives by capillary electrophoresis, J. Sep. Sci. 32 (2009) 1087–1095.
[54] N. Pourreza, S. Rastegarzadeh, A. Larki, Nano-TiO_2 modified with 2-mercapto-benzimidazole as an efficient adsorbent for removal of Ag(I) from aqueous solutions, J. Ind. Eng. Chem. 20 (2014) 127–132.
[55] P. Sorlier, A. Denuzière, C. Viton, A. Domard, Relation between the degree of acetylation and the electrostatic properties of chitin and chitosan, Biomacromolecules 2 (2001) 765–772.
[56] F.A.R. Pereira, K.S. Sousa, G.R.S. Cavalcanti, D.B. França, L.N.F. Queiroga, I.M.G. Santos, M.G. Fonseca, M. Jaber, Green biosorbents based on chitosan-montmorillonite beads for anionic dye removal, J. Environ. Chem. Eng. 5 (2017) 3309–3318.
[57] S. Sharma, M. Barathi, N. Rajesh, Efficacy of a heterocyclic ligand anchored biopolymer adsorbent for the sequestration of palladium, Chem. Eng. J. 259 (2015) 457–466.
[58] M.L. Duarte, M.C. Ferreira, M.R. Marvao, J. Rocha, An optimised method to determine the degree of acetylation of chitin and chitosan by FTIR spectroscopy, Int. J. Biol. Macromol. 31 (2002) 1–8.
[59] Z. Zhou, F. Jiang, T.-C. Lee, T. Yue, Two-step preparation of nano-scaled magnetic chitosan particles using Triton X-100 reversed-phase water-in-oil microemulsion system, J. Alloys Compd. 581 (2013) 843–848.
[60] M. Edraki, D. Zaarei, Modification of montmorillonite clay with 2-mercapto-benzimidazole and investigation of their antimicrobial properties, 2 (2018) 189-200.
[61] S. Wang, D. Yu, Adsorption of Cd(II), Pb(II), and Ag(I) in aqueous solution on hollow chitosan microspheres, J. Appl. Polym. Sci. 118 (2010) 733–739.
[62] K.L.M. Taaca, H. Nakajima, K. Thumanu, P. Janphuang, N. Chanlek, M.R. Vasquez,

Spectroscopic studies of plasma-modified silver-exchanged zeolite and chitosan composites, Mater. Chem. Phys., 250 (2020) Art. N° 122980.
[63] F.G. Helfferich, Ion Exchange, Dover Publications Inc, New York, NY (USA), 1995, p. 631.
[64] M.H. Entezari, T. Soltani, Simultaneous removal of copper and lead ions from a binary solution by sono-sorption process, J. Hazard. Mater. 160 (2008) 88–93.
[65] A. Mary Ealias, M.P. Saravanakumar, A critical review on ultrasonic-assisted dye adsorption: Mass transfer, half-life and half-capacity concentration approach with future industrial perspectives, Crit. Rev. Env. Sci. Technol. 49 (2019) 1959–2015.
[66] S. Sarkar, M. Sarkar, Ultrasound assisted batch operation for the adsorption of hexavalent chromium onto engineered nanobiocomposite, Heliyon, 5 (2019) Art. N° e01491.
[67] M. Behbahani, V. Zarezade, A. Veisi, F. Omidi, S. Bagheri, Modification of magnetized MCM-41 by pyridine groups for ultrasonic-assisted dispersive micro-solid-phase extraction of nickel ions, Int. J. Environ. Sci. Technol. 16 (2019) 6431–6440.
[68] J.-P. Simonin, On the comparison of pseudo-first order and pseudo-second order rate laws in the modeling of adsorption kinetics, Chem. Eng. J. 300 (2016) 254–263.
[69] M.A. Hubbe, S. Azizian, S. Douven, Implications of apparent pseudo-second-order adsorption kinetics onto cellulosic materials: a review, 2019, 14 (2019) 45.
[70] W.-B. Zhang, M. Deng, C.-X. Sun, S.-B. Wang, Ultrasound-enhanced adsorption of chromium(VI) on Fe_3O_4 magnetic particles, Ind. Eng. Chem. Res. 53 (2014) 333–339.
[71] K. Furukawa, Y. Takahashi, H. Sato, Effect of the formation of EDTA complexes on the diffusion of metal ions in water, Geochim. Cosmochim. Acta 71 (2007) 4416–4424.
[72] M.A. Al-Ghouti, D.A. Da'ana, Guidelines for the use and interpretation of adsorption isotherm models: A review, J. Hazard. Mater., 393 (2020) Art. N°122383.
[73] S. Bhattarai, J.S. Kim, Y.-S. Yun, Y.-S. Lee, Preparation of polyaniline-coated polystyrene nanoparticles for the sorption of silver ions, React. Funct. Polym. 105 (2016) 52–59.
[74] X.-G. Li, H. Feng, M.-R. Huang, Redox sorption and recovery of silver ions as silver nanocrystals on poly(aniline-co-5-sulfo-2-anisidine) nanosorbents, Chem. Eur. J. 16 (2010) 10113–10123.
[75] J. Wang, W. Zhang, X. Kang, C. Zhang, Rapid and efficient recovery of silver with nanoscale zerovalent iron supported on high performance activated carbon derived from straw biomass, Environ. Pollut., 255 (2019) Art. N° 113043.
[76] A.D. Dwivedi, S.P. Dubey, M. Sillanpaa, H. Liimatainen, T. Suopajarvi, J. Niinimaki, Y.-N. Kwon, C. Lee, Distinctive green recovery of silver species from modified cellulose: mechanism and spectroscopic studies, Int. J. Biol. Macromol. 76 (2015) 109–118.
[77] P.S. Ghosal, A.K. Gupta, Determination of thermodynamic parameters from Langmuir isotherm constant-revisited, J. Mol. Liq. 225 (2017) 137–146.
[78] E.C. Lima, A. Hosseini-Bandegharaei, J.C. Moreno-Piraján, I. Anastopoulos, A critical review of the estimation of the thermodynamic parameters on adsorption equilibria. Wrong use of equilibrium constant in the Van't Hoof equation for calculation of thermodynamic parameters of adsorption, J. Mol. Liq. 273 (2019) 425–434.
[79] M.H. Morcali, B. Zeytuncu, S. Akman, O. Yucel, Preparation and sorption behavior of DEAE-cellulose-thiourea-glutaraldehyde sorbent for Pt(IV) and Pd(II) from leaching solutions, Desalin. Water Treat. 57 (2016) 6582–6593.
[80] W. Zhang, L. Wu, X. Han, L. Yao, S. Zhao, J. Sun, Y. Xu, J. Li, C. Xiong, Green chemical synthesis of new chelating fiber and its mechanism for recovery gold from aqueous solution, J. Hazard. Mater., 378 (2019) Art. N° 120674.
[81] J. Son, Y. Hong, G. Han, T.S. Nguyen, C.T. Yavuz, J.-I. Han, Gold recovery using porphyrin-based polymer from electronic wastes: Gold desorption and adsorbent regeneration, Sci. Total Environ., 704 (2020) Art. N° 135405.
[82] P. Lukinskas, I. Savickaja, V. ŠukienĖ, A. Lukinskas, Potentiometric study of silver complexes with thiourea in acid media, J. Coord. Chem. 61 (2008) 2528–2535.
[83] S.E. Livingstone, Metal complexes of ligands containing sulphur, selenium, or tellurium as donor atoms, Quarterly Reviews, Chemical Society 19 (1965) 386–425.
[84] M.D. Đurović, R. Puchta, Ž.D. Bugarčić, R. van Eldik, Studies on the reactions of $[AuCl4]^-$ with different nucleophiles in aqueous solution, Dalton Trans. 43 (2014) 8620–8632.
[85] M.E. Poisot Díaz, A.R. Alonso, I. González, G.T. Lapidus, Influence of oxygen reduction and hydrogen evolution in the gold and silver direct electrodeposition process from thiourea solutions in a filter press type reactor, Hydrometallurgy, 129-130 (2012) 90-96.
[86] J. Zolgharnein, A. Shahrjerdi, N. Asanjarani, G. Azimi, Highly efficient and selective transport of Au(III) through a bulk liquid membrane using potassium-dicyclohexyl-18-crown-6 as carrier, Sep. Sci. Technol. 43 (2008) 3119–3133.
[87] R.G. Pearson, Acids and bases, Science (New York, N.Y.), 151 (1966) 172-177.
[88] J.C. Moreira, L.C. Pavan, Y. Gushikem, Adsorption of Cu(II), Zn(II), Cd(II), Hg(II) and Pb(II) from aqueous solutions on a 2-mercaptobenzimidazole-modified silica gel, Microchim. Acta 102 (1990) 107–115.
[89] W. Lee, S.-E. Lee, C.-H. Lee, Y.-S. Kim, Y.-I. Lee, A chelating resin containing 1-(2-thiazolylazo)-2-naphthol as the functional group; synthesis and sorption behavior for trace metal ions, Microchem. J. 70 (2001) 195–203.
[90] R. Saha, S. Das, A. Banerjee, A. Sahana, M. Sudarsan, A.M.Z. Slawin, Y. Li, D. Das, pH dependent separation of uranium by chelation chromatography using pyridine 2,6-dimethanol as a chelator: Single crystal X-ray structural confirmation of the chelated uranium complex, J. Hazard. Mater. 181 (2010) 154–160.
[91] M. Truskolaska, K. Jankowski, Selective non-chromatographic determination of tributyltin in sediments using EDTA and diphenylcarbazone as masking agent, Int. J. Environ. Anal. Chem. 98 (2018) 295–307.
[92] M.N. Kouraim, M.S. Hagag, A.H. Ali, Sorption of uranium from radioactive wastes by silicate-neutralised polyacrylic, Int. J. Environ. Anal. Chem. 100 (2020) 825–840.
[93] H. Dozol, G. Mériguet, B. Ancian, V. Cabuil, H. Xu, D. Wang, A. Abou-Hassan, On the synthesis of Au nanoparticles using EDTA as a reducing agent, J. Phys. Chem. C 117 (2013) 20958–20966.
[94] M. Deschatre, F. Ghillebaert, J. Guezennec, C.S. Colin, Sorption of copper(II) and silver(I) by four bacterial exopolysaccharides, Appl. Biochem. Biotechnol. 171 (2013) 1313–1327.
[95] Y. Pei, X. Chen, D. Xiong, S. Liao, G. Wang, Removal and recovery of toxic silver ion using deep-sea bacterial generated biogenic manganese oxides, PLoS One, 8 (2013) Art. N° 0081627.
[96] U. Condomitti, A.T. Silveira, G.W. Condomitti, S.H. Toma, K. Araki, H.E. Toma, Silver recovery using electrochemically active magnetite coated carbon particles, Hydrometallurgy 147 (2014) 241–245.
[97] G. Kiani, M. Soltanzadeh, High capacity removal of silver(I) and lead(II) ions by modified polyacrylonitrile from aqueous solutions, Desalin. Water Treat. 52 (2014) 3206–3218.
[98] G.Z. Kyzas, D.N. Bikiaris, Characterization of binding properties of silver ion-imprinted polymers with equilibrium and kinetic models, J. Mol. Liq. 212 (2015) 133–141.
[99] F.V. Silva-Medeiros, N. Consolin-Filho, M. Xavier de Lima, F.P. Bazzo, M.A.S.D. Barros, R. Bergamasco, C.R.G. Tavares, Kinetics and thermodynamics studies of silver ions adsorption onto coconut shell activated carbon, Environ. Technol. 37 (2016) 3087–3093.
[100] C. Jeon, Adsorption and recovery of immobilized coffee ground beads for silver ions from industrial wastewater, J. Ind. Eng. Chem. 53 (2017) 261–267.
[101] M.R. Salvadori, R.A. Ando, C.A. Oller Nascimento, B. Correa, Dead biomass of Amazon yeast: a new insight into bioremediation and recovery of silver by intracellular synthesis of nanoparticles, J. Environ. Sci. Health., Part A 52 (2017) 1112–1120.
[102] P. Staron, J. Chwastowski, M. Banach, Sorption and desorption studies on silver ions from aqueous solution by coconut fiber, J. Cleaner Prod. 149 (2017) 290–301.
[103] R. Taheri, N. Bahramifar, M.R. Zarghami, H. Javadian, Z. Mehraban, Nanospace engineering and functionalization of MCM-48 mesoporous silica with dendrimer amines based on 1,3,5 -triazines for selective and pH-independent sorption of silver ions from aqueous solution and electroplating industry wastewater, Powder Technol. 321 (2017) 44–54.
[104] H. Shehzad, E. Ahmed, A. Sharif, M.I. Din, Z.H. Farooqi, I. Nawaz, R. Bano, M. Iftikhar, Amino-carbamate moiety grafted calcium alginate hydrogel beads for effective biosorption of Ag(I) from aqueous solution: Economically-competitive recovery, Int. J. Biol. Macromol. 144 (2020) 362–372.